© 2022. Published by The Company of Biologists Ltd | Development (2022) 149, dev200236. doi:10.1242/dev.200236

RESEARCH ARTICLE

Lmo7 recruits myosin II heavy chain to regulate actomyosin contractility and apical domain size in *Xenopus* ectoderm

Miho Matsuda*, Chih-Wen Chu and Sergei Y. Sokol

ABSTRACT

Apical constriction, or a reduction in size of the apical domain, underlies many morphogenetic events during development. Actomyosin complexes play an essential role in apical constriction; however, the detailed analysis of molecular mechanisms is still pending. Here, we show that Lim domain only protein 7 (Lmo7), a multidomain adaptor at apical junctions, promotes apical constriction in the *Xenopus* superficial ectoderm, whereas apical domain size increases in Lmo7-depleted cells. Lmo7 is primarily localized at apical junctions and promotes the formation of the dense circumferential actomyosin belt. Strikingly, Lmo7 binds non-muscle myosin II (NMII) and recruits it to apical junctions and the apical cortex. This NMII recruitment is essential for Lmo7-mediated apical constriction. Lmo7 knockdown decreases NMIIA localization at apical junctions and delays neural tube closure in *Xenopus* embryos. Our findings suggest that Lmo7 serves as a scaffold that regulates actomyosin contractility and apical domain size.

KEY WORDS: Lmo7, Actomyosin contractility, Non-muscle myosin II, Adherens junctions, Morphogenesis, *Xenopus ectoderm*

INTRODUCTION

Apical constriction, or reduction in size of the apical domain, underlies a variety of morphogenetic processes during embryonic development (Martin and Goldstein, 2014; Perez-Vale and Peifer, 2020; Sawyer et al., 2010). One consequence of apical constriction is the cell delamination required for epithelial-to-mesenchymal transition (EMT) (Ramkumar et al., 2016; Williams et al., 2012). Another consequence is tissue invagination that leads to epithelial furrow or tube formation (Eiraku et al., 2011; Sherrard et al., 2010; Wallingford et al., 2013). Significantly, failure of apical constriction results in epithelial morphogenesis defects, such as abnormal neural tube closure (Balashova et al., 2017; Brown and Garcia-Garcia, 2018; Colas and Schoenwolf, 2001; Haigo et al., 2003; Itoh et al., 2014; Kowalczyk et al., 2021).

The actomyosin system that drives apical constriction is a highly dynamic network of filamentous actin (F-actin) and non-muscle myosin II (NMII), crosslinked by α-actinin (Murphy and Young, 2015; Vicente-Manzanares et al., 2009). NMII heavy chains assemble tail-to-tail into bipolar filaments that form NMII mini-filaments (Bresnick, 1999; Heissler and Sellers, 2014; Shutova and Svitkina, 2018). The head domains of NMII mini-filaments bind F-actin and the sliding movements between F-actin and NMII generate contractile forces (Lecuit et al., 2011; Martin and Goldstein, 2014; Salbreux et al., 2012). Actomyosin networks can be arranged in many patterns, from loose mesh-like networks to highly organized sarcomere-like actomyosin bundles (Agarwal and Zaidel-Bar, 2019; Schwayer et al., 2016).

Two models have been proposed to explain how actomyosin networks regulate apical constriction in epithelial cells. The 'purse-string' model involves circumferential actomyosin bundles that run parallel to apical junctions (Boller et al., 1985; Coravos and Martin, 2016; Gorfinkiel and Blanchard, 2011; Hirano et al., 1987; Munjal et al., 2015; Yonemura et al., 1995). These bundles are linked to apical junctions by F-actin-binding proteins, including αE-catenin, vinculin and afadin at adherens junctions (AJs), and zonula occludens proteins (ZO-1-3) at tight junctions (TJs) (Abe and Takeichi, 2008; Drees et al., 2005; Fanning et al., 1998; Itoh et al., 1997; Sawyer et al., 2009; Yamada et al., 2005). NMII motor activity pulls antiparallel F-actin arrays and reduces the distance between sarcomere-like repeats. The other mechanism involves medioapical actomyosin meshwork that is also linked to apical junctions but generates pulling forces perpendicular to these junctions (Azevedo et al., 2011; Blanchard et al., 2010; David et al., 2010; Martin et al., 2009; Mason et al., 2013). In both models, the association of actomyosin network and apical junctions is essential for apical constriction, because the uncoupling leads to failure of apical constriction in *canoe/afadin*-deficient *Drosophila* embryos (Roh-Johnson et al., 2012; Sawyer et al., 2011, 2009).

To gain further insights into the interaction of the actomyosin network with apical junctional machinery, we initiated the study of LIM domain only protein 7 (Lmo7) that was originally identified as a binding partner of afadin and α-actinin (Ooshio et al., 2004). Although mice lacking *Lmo7* are viable and develop relatively minor defects (Du et al., 2019; Lao et al., 2015; Mull et al., 2015; Tanaka-Okamoto et al., 2009), Lmo7 has been implicated in skeletal and cardiac muscle differentiation, and in metastatic cancer (He et al., 2018; Holaska et al., 2006; Liu et al., 2021; Nakamura et al., 2011; Ott et al., 2008). Notably, the *Drosophila* homologue Smallish is essential for epithelial morphogenesis and controls apical domain size in the follicular epithelium (Beati et al., 2018). These observations suggest that Lmo7 may have uncharacterized functions in the reorganization of actomyosin and apical junctions in vertebrate epithelia.

This study describes Lmo7 as a novel regulator of actomyosin contractility and apical constriction in *Xenopus* ectoderm cells. This activity of Lmo7 requires the Rho-ROCK-NMII system and the primary function of Lmo7 appears to be the binding and recruitment of NMII heavy chain to the actomyosin networks in the apical region of cells. Lmo7 knockdown delays neural tube closure in *Xenopus* embryos. We propose that Lmo7 is a scaffold protein that regulates crosstalk between apical junctions and the actomyosin system.

Department of Cell, Developmental and Regenerative Biology, Icahn School of Medicine at Mount Sinai, New York, NY 10029, USA.

*Author for correspondence (miho.matsuda@mssm.edu)

M.M., 0000-0002-7495-5905; S.Y.S., 0000-0002-3963-9202

Handling Editor: Steve Wilson
Received 28 September 2021; Accepted 30 March 2022

Development (2022) 149, dev200236. doi:10.1242/dev.200236

RESULTS

Lmo7 is localized in the proximity of apical cell junctions in *Xenopus* ectoderm

To understand Lmo7 function in epithelial morphogenesis, we studied Lmo7 protein distribution in *Xenopus* ectoderm, a tissue that exhibits dynamic remodeling of apical junctions (Higashi et al., 2016). In stage 11 ectoderm, Lmo7 localized at cell-cell boundaries (Fig. 1A). Ectoderm cryosections confirmed Lmo7 apicolateral distribution to the area corresponding to apical junctions (arrowheads in Fig. 1C,C'). This distribution was different from the localization of other components of apical junctions. First, Lmo7 was visible as two distinct parallel bands along cell-cell boundaries, especially in short cell contact areas (Fig. 1B). By contrast, ZO-1, a tight junction (TJ) component, and β-catenin, a adherens junction (AJ) component (Hartsock and Nelson, 2008), were detected as a single band flanked by two Lmo7 bands (Fig. 1D-H′). Second, Lmo7 accumulated near but not at tricellular junctions (Fig. 1B′). These observations establish the localization of Lmo7 in the proximity of apical junctions. In addition to apical junctions, Lmo7 puncta were visible at the apical cortex (arrowheads in Fig. 1F,F″).

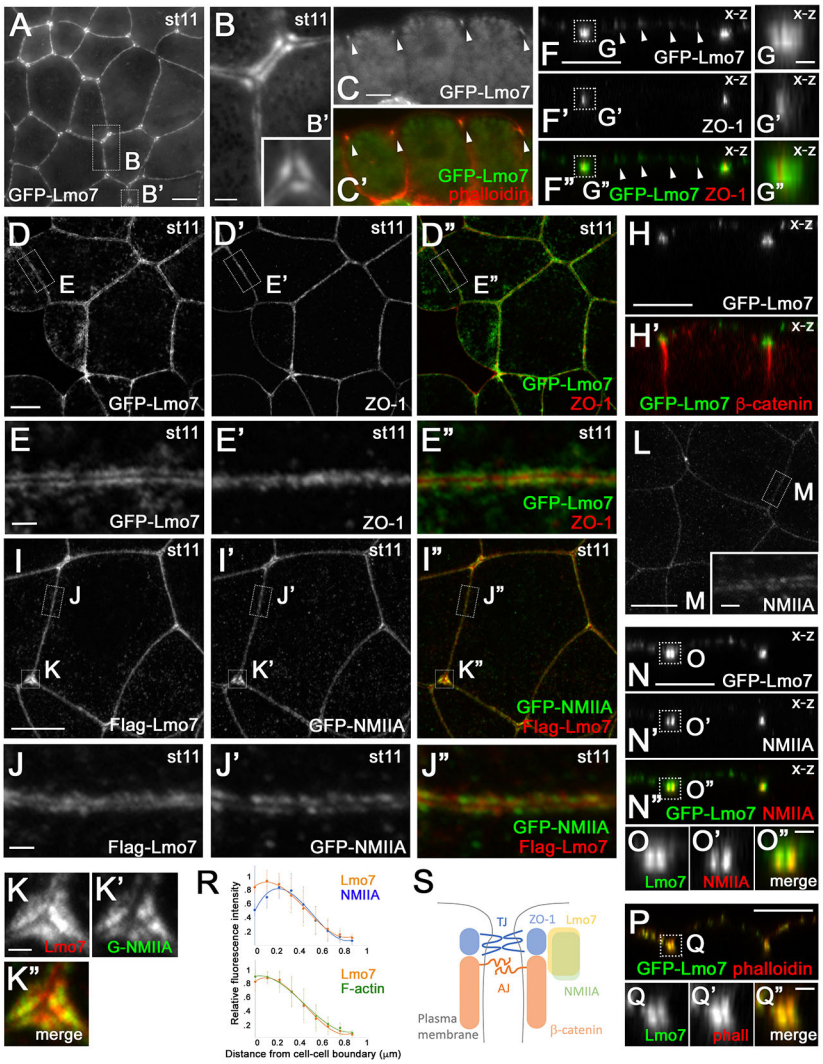

Fig. 1. Lmo7 localizes at junctional actomyosin bundles in *Xenopus* ectoderm cells. (A-Q″) *Xenopus* embryos were injected into animal blastomeres with GFP-Lmo7 or Flag-Lmo7 RNA (200 pg) or GFP-NMIIA RNA (300 pg) as indicated and the superficial ectoderm was imaged at stage 11. Protein localization was evaluated by direct GFP fluorescence, or by indirect immunofluorescence for Flag-Lmo7, endogenous NMIIA, ZO-1 and β-catenin. (A) Peri-junctional GFP-Lmo7 localization. Areas marked by rectangles are enlarged in B and B′. (B) Peri-junctional double bands of GFP-Lmo7 are more evident in shorter cell-cell junctions. (B′) GFP-Lmo7 is enriched near tricellular junctions but excluded from them. (C,C′) Cryosections of the superficial layer of ectoderm showing GFP-Lmo7 localization at the most apical region of the lateral membrane (arrowheads), co-stained with phalloidin. (D-G″) Relative distribution of GFP-Lmo7 and endogenous ZO-1 in *x-y* view (D-E″) and *x-z* view (F-G″). Areas marked by rectangles in D-D″ and F-F″ are enlarged in E-E″ and G-G″, respectively. (H,H′) Relative localization of GFP-Lmo7 and endogenous β-catenin in *x-z* view. (I-J″) Relative localization of Flag-Lmo7 and GFP-NMIIA. Bi-cellular junctions and tricellular junctions marked by rectangles and squares in I-I″ are enlarged in J-J″ and K-K″, respectively. (L,M) Endogenous NMIIA localization. An area marked by a rectangle is enlarged in M. (N-O″) Relative localization of GFP-Lmo7 and endogenous NMIIA in *x-z* view. Areas marked by rectangles in N-N″ are enlarged in O-O″. (P-Q″) Relative localization of GFP-Lmo7 and F-actin. An area marked by a rectangle in P is enlarged in Q-Q″. (R) Quantification of GFP-Lmo7, NMIIA and F-actin fluorescence intensity near apical junctions. The cell-cell boundary is defined as 0 on the *x*-axis. GFP-Lmo7 is located closer to the cell-cell boundary (0.138 μm) than NMIIA (0.272 μm) (upper panel, n=28, P<0.001). There is no statistically significant difference between GFP-Lmo7 (0.139 μm) and F-actin (0.101 μm) (lower panel, n=16, P>0.25). Spearman's correlation coefficient is 0.9959 and 0.9879 in GFP-Lmo7 and NMIIA in the upper panel, and 0.9943 and 0.9968 in GFP-Lmo7 and F-actin in the lower panel. (S) Schematics of the relative distribution of Lmo7 in apical junctions. Scale bars: 10 μm in A,C,D,F,H,I,L,N,P; 2 μm in B,E,G,J,K,M, O,Q. Images shown are representative of two to five experiments.

Development (2022) 149, dev200236. doi:10.1242/dev.200236

We next asked whether Lmo7 localization at the cell-cell boundaries corresponds to the circumferential actomyosin bundles that run parallel to apical junctions (Yonemura et al., 1995). The major components of actomyosin bundles are F-actin, NMII and α-actinin. We observed that both exogenous GFP-NMIIA (Fig. 1I′,J′) and endogenous NMIIA (Fig. 1L,M,N′,O′) form two bands along the cell-cell boundaries. Lmo7 was positioned in a way largely overlapping with the NMIIA bands (Fig. 1I-J″,N-O″), but somewhat closer to the plasma membrane at both bicellular (Fig. 1J-J″,O-O″,R) and tricellular (Fig. 1K-K″) junctions. In addition, Lmo7 double line closely overlapped with phalloidin staining (Fig. 1P-R). These findings document Lmo7 localization at peri-junctional actomyosin bundles (Fig. 1S).

Lmo7 induces apical constriction in *Xenopus* superficial ectoderm

A previous study showed that Smallish, the Lmo7 homologue in *Drosophila*, caused apical domain reduction in follicular epithelial cells (Beati et al., 2018). We therefore asked whether Lmo7 has a similar activity. Injection of GFP-Lmo7 RNA triggered hyperpigmentation and invagination of ectoderm at the site of injection (Fig. 2A,B). Because pigment granule accumulation is commonly associated with apical F-actin bundle formation in *Xenopus* ectoderm (Kurth and Hausen, 2000), increased pigmentation serves as a good indicator of apical constriction (Haigo et al., 2003; Itoh et al., 2014; Merriam et al., 1983; Morita et al., 2010; Ossipova et al., 2014; Popov et al., 2018). In addition, we confirmed apical constriction by measuring apical domains *en face* (Fig. 2C,D) and by assessing the ratio of apical width to basolateral length of cells in cross-sections (Fig. 2E-G) after phalloidin co-staining. To deplete Lmo7, a translation-blocking morpholino oligonucleotide (*lmo7*-ATGMO) was injected in the ectoderm. Although no overt effect on ectoderm pigmentation was apparent, *lmo7* knockdown expanded the apical domain (Fig. 2H-I). This effect of *lmo7*MO was rescued by co-injection of GFP-Lmo7 RNA (Fig. S1). This is consistent with the Lmo7 function in apical domain size regulation.

Reorganization of the apical actomyosin network by Lmo7

A highly organized actomyosin network is known to generate the contractile force required for apical constriction. We compared peri-junctional actomyosin bundles in Lmo7-expressing and control non-expressing cells (Fig. 3). Lmo7-expressing cells exhibited thick double bands of Flag-Lmo7 in a sarcomere-like pattern (Fig. 3A,C). The effect was less pronounced in embryos injected with lower dose of *lmo7* RNA (Fig. 1E,J), suggesting dose-dependent effects. Flag-Lmo7 induced the formation of intense F-actin double bands that largely overlapped with Lmo7 (Figs 3A-D and 1P-Q″). The appearance of thick F-actin bundles was accompanied by the accumulation of phosphorylated myosin regulatory light chain (pMRLC) (Fig. 3E-H), NMIIA (Fig. 3I-L) and exogenous α-actinin 4 (Fig. S2). These results suggest that Lmo7 promotes actomyosin bundle formation at apical junctions.

We next examined Lmo7 effects on the medioapical actomyosin network that may also contribute to apical constriction in *Xenopus* ectoderm (Arnold et al., 2019). A small fraction of Lmo7 localized to the medioapical cortex and formed puncta (Fig. 4A,C). These GFP-Lmo7 puncta colocalized with puncta of F-actin (Fig. 4C-D″) and NMIIA (Fig. 4E-F″). More apical puncta formed in cells expressing high amounts of Lmo7, indicating dose dependency (Fig. 4A-D″,G). Taken together, these results suggest that Lmo7

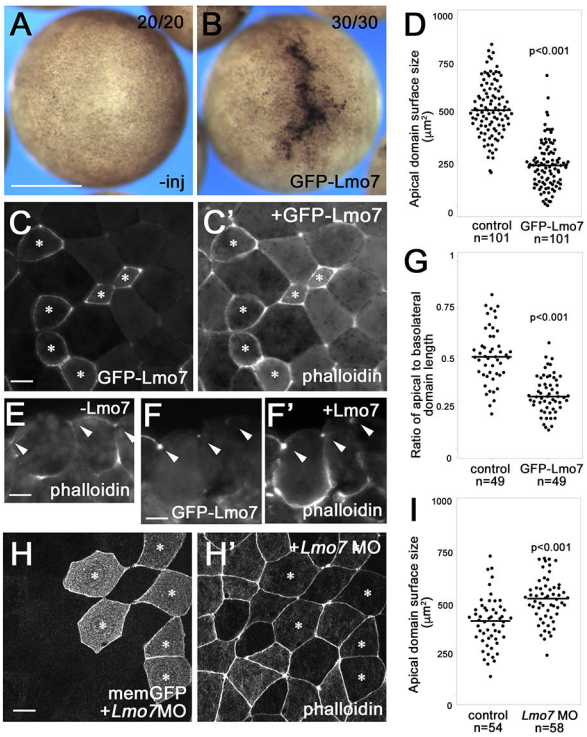

Fig. 2. Lmo7 induces apical constriction in *Xenopus* ectoderm. (A,B) GFP-Lmo7 RNA (1 ng) was injected into two animal blastomeres of four- to eight-cell stage embryos. (A) Control uninjected embryo at stage 11. (B) Embryo expressing GFP-Lmo7 at stage 11 exhibiting apical pigment granule accumulation. (C,C′) Reduced apical domain in cells expressing GFP-Lmo7 (200 pg RNA) in stage 11 embryos. *En face* view of the ectoderm co-stained with phalloidin. Asterisks indicate GFP-Lmo7-expressing cells. (D) Quantification of apical domain surface size in cells expressing GFP-Lmo7 (n=101) and adjacent control cells (n=101). Images were taken from at least five embryos. (E-F′) Cross-sections of the ectoderm in stage 11 embryos expressing GFP-Lmo7 RNA (200 pg). Embryos were co-stained with phalloidin. Arrowheads indicate GFP-Lmo7 or F-actin accumulation at the most apical region of the basolateral membrane. (G) The ratio of the apical to the basolateral domain length in the cells expressing GFP-Lmo7 (n=49) and uninjected control cells (n=49). (H,H′) Increased apical domain in Lmo7-ATGMO cells. Lmo7-ATGMO (30 ng) was co-injected with membrane-tethered RNA (100 pg). The ectoderm from stage 11 embryos was co-stained with phalloidin, *en face* view. Asterisks indicate Lmo7-ATGMO-containing cells. (I) Quantification of apical domain size in Lmo7-ATGMO cells (n=58) and adjacent control cells (n=54). Images were taken from at least five embryos. Statistical significance of the difference between the median values was assessed by the Mann–Whitney U-test. Scale bars: 500 µm in A; 10 µm in C,E, F,H. Images shown are representative of two or three experiments.

increases the density of the actomyosin network both at apical junctions and the medioapical cortex.

The Rho-ROCK-NMII pathway is required for Lmo7-mediated apical constriction

Rho-ROCK-NMII signaling has been shown to play a crucial role in apical constriction. The main outcome of this pathway is the phosphorylation of myosin regulatory light chains (MRLCs) by Rho-dependent protein kinase (ROCK) (Das et al., 2014; Haigo et al., 2003; Hildebrand, 2005; Hildebrand and Soriano, 1999; Itoh et al., 2014; Nakajima and Tanoue, 2011; Nakajima and Tanoue, 2012; Nishimura and Takeichi, 2008; Popov et al., 2018). To test whether the Lmo7 effect on *Xenopus* ectoderm requires the Rho-ROCK-NMII pathway, we inhibited MRLC phosphorylation by the co-expression of a dominant-interfering form of ROCK (ROK-C) or

Development (2022) 149, dev200236. doi:10.1242/dev.200236

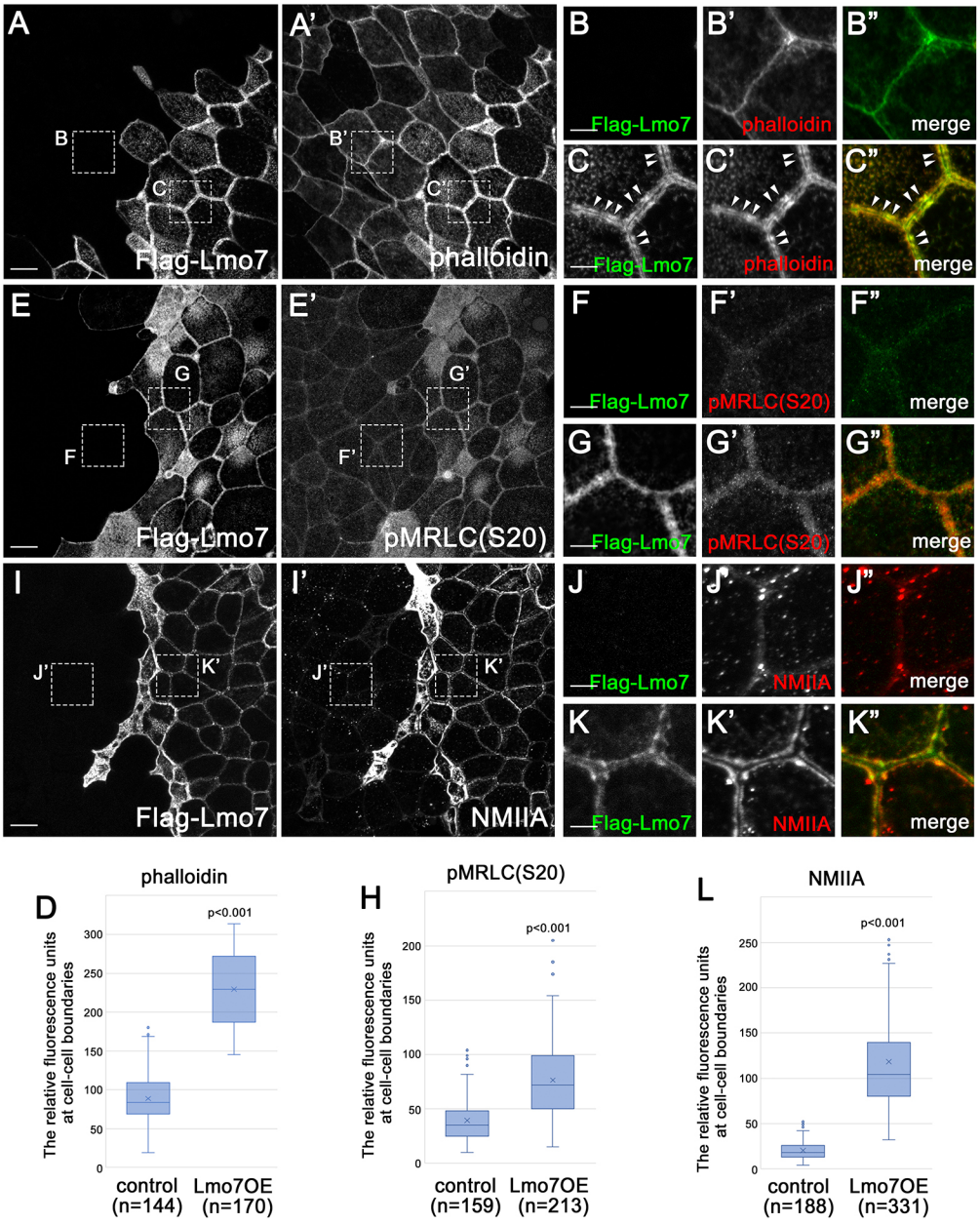

Fig. 3. Lmo7 promotes actomyosin bundle formation at apical junctions. Effects of Flag-Lmo7 overexpression on peri-junctional actomyosin networks. Flag-Lmo7 RNA (1 ng) was injected into one blastomere of four- to eight-cell stage embryos. Stage 11 embryos were co-stained with phalloidin, anti-Flag, anti-pMRLC or anti-NMIIA antibodies, as indicated. The superficial ectoderm was imaged. (A-C″) F-actin bundle formation in cells expressing Flag-Lmo7. Areas marked by rectangles in A, A′ are enlarged in B-C″. (C-C″) Lmo7 double bands between two adjacent Flag-Lmo7-expressing cells overlap with F-actin double bands. There are periodic sarcomere-like structures (arrowheads). (D) Phalloidin fluorescence intensity was measured at the borders between two adjacent control cells (control) or two Lmo7-expressing cells (Lmo7OE). (E-G″) MRLC phosphorylation at Ser 20. Areas marked by rectangles in E-E′ are enlarged in F-G″. (H) Fluorescence intensity of pMRLC(S20) staining related to images in E-G″. (I-K″) NMIIA accumulation. Areas marked by rectangles are enlarged in J-K″. (L) Fluorescence intensity of NMIIA staining related to images in I-K″. The boxes and whiskers indicate the lower and upper quartiles, and variability outside the upper and lower quartiles. Statistical significance of the difference was assessed by the Mann–Whitney U-test. Scale bars: 10 µm in A,E,I; 2 µm in B,C,F,G,J,K. Images shown are representative of two to four experiments.

constitutively active myosin phosphatase Mypt1 (Mypt1CA) (Feng et al., 1999; Marlow et al., 2002; Weiser et al., 2009). Apical constriction was assessed by pigment granule accumulation (Fig. 5A-D) and the quantification of apical domain size (Fig. 5E-G). Co-expression of either RNA suppressed Lmo7-mediated apical constriction (Fig. 5C,D,F,G), indicating that Rho-ROCK-NMII pathway is required for this process.

The phosphorylation of MRLC promotes NMII bipolar filament formation and NMII binding to anti-parallel F-actin, and may initiate force generation. We therefore asked whether Lmo7-mediated actomyosin reorganization increases mechanical tension at apical junctions and/or the apical cortex. We took advantage of Ajuba family proteins that change their localization in response to tension (Chu et al., 2018; Ibar et al., 2018; Rauskolb et al., 2014; Razzell et al., 2018). One of the Ajuba family proteins, Wilms tumor 1-interacting protein (Wtip), forms aggregates or puncta. These puncta disappear in cells expressing Shroom3, a known inducer of apical constriction, potentially reflecting the increased tension at the cell cortex (Chu et al., 2018). We injected Flag-Lmo7 RNA in a subpopulation of RFP-HA-Wtip-expressing cells (Fig. 5H). The RFP-HA-Wtip puncta both at the apical cortex (Fig. 5L) and apical junctions (Fig. 5M) were no longer visible in Lmo7-expressing cells when compared with the non-expressing control cells (Fig. 5I-M). Whereas mechanisms and physiological significance of Wtip puncta formation warrant further investigation, these results suggest that Lmo7 increases tension in overexpressing cells.

Determination of the domains required for Lmo7-mediated apical constriction

Lmo7 has the calponin homology domain (CH), the domain of unknown function DUF4757, the α-actinin-binding region (Ooshio et al., 2004), the PDZ domain, two coiled-coil domains and the LIM domain that binds to afadin (Ooshio et al., 2004) (Fig. 6A). To define the domains of Lmo7 required for apical constriction, various Lmo7 constructs were expressed in the superficial ectoderm (Fig. S3). We found that the removal of the C-terminal LIM

Development (2022) 149, dev200236. doi:10.1242/dev.200236

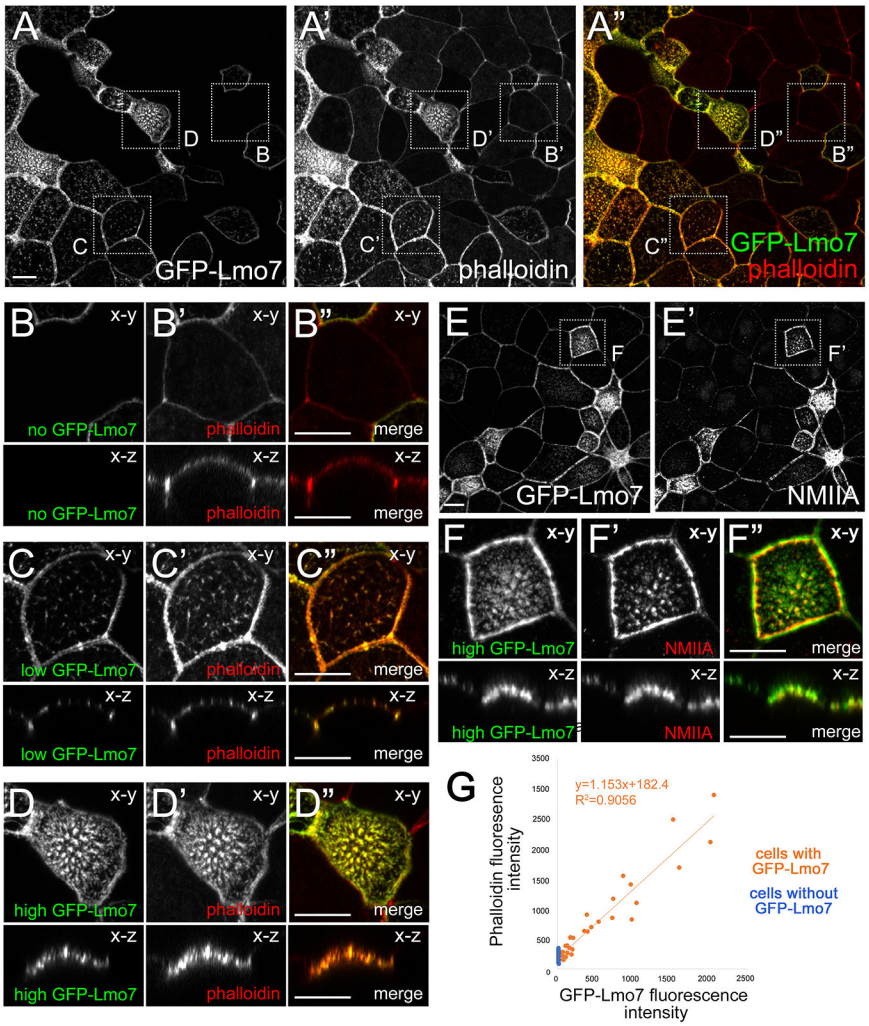

Fig. 4. Lmo7 promotes actomyosin bundle formation at the medioapical cortex. GFP-Lmo7 RNA (1 ng) was injected into one blastomere of four- to eight-cell stage embryos. Images show the superficial ectoderm of stage 11 embryos co-stained with phalloidin or NMIIA antibodies. (A-D″) F-actin accumulation at the medioapical cortex in cells expressing GFP-Lmo7. Areas marked by rectangles in A-A″ are enlarged in B-D″. *x-y* views and *x-z* views are shown for uninjected cells (B-B″) and cells expressing low (C-C″) and high (D-D″) levels of GFP-Lmo7. (E-F″) NMIIA accumulation at the medioapical cortex in GFP-Lmo7-expressing cells. Areas marked by rectangles are enlarged in F-F″. *x-y* view and *x* view are shown. (G) Quantification of medioapical GFP-Lmo7 and F-actin related to images in A-D″. Fluorescence intensities of medioapical GFP-Lmo7 (*x*-axis) and phalloidin (*y*-axis) are shown. Each dot represents one cell. GFP-Lmo7 increases the accumulation of F-actin at the medioapical cortex in a dose-dependent manner. Scale bars: 10 µm. Images shown are representative of two to four experiments.

domain (Fig. 6B), the coiled-coil domain and the PDZ domain (Fig. 6C), or the N-terminal CH domain (Fig. 6F) did not affect the pigment granule accumulation. On the other hand, the α-actinin-binding region was necessary for this activity (Fig. 6D,E). DUF4757(aa 242-400) was also necessary (Fig. 6G) but not sufficient on its own (Fig. 6I). Lmo7(aa 242-709) containing both DUF4757 and the α-actinin-binding region was the shortest fragment that triggered apical pigment accumulation (Fig. 6H). We confirmed that Lmo7(aa 242-709), but not Lmo7(aa 242-400), reduced apical domain size in individual cells (Fig. 6K-M). These studies suggest that the Lmo7(aa 242-709) was both required and sufficient for apical constriction.

Lmo7 binds and recruits NMII to apical junctions via DUF4757

We next evaluated whether Lmo7 interacts with NMII heavy chain as reported for its paralog human Limch1 (Lin et al., 2017). Both endogenous NMIIA and NMIIB were found in Flag-Lmo7 pull-downs in transfected HEK293T cells (Fig. 7A). As DUF4757(aa 242-400) was required and sufficient for this binding (Fig. 7A), we will refer to it as the NMII-binding domain (NMIIBD). These results suggest that Lmo7 effect on actomyosin may be due to the NMIIBD interaction with NMII heavy chains. Consistent with our hypothesis, alanine substitution of the conserved WQ-WK amino acids in NMIIBD (Fig. 7B) eliminated the binding of NMIIA and IIB in HEK293T cells (Fig. S4A). Flag-Lmo7(AAAA) localized at apical junctions (Fig. 8A,B) but did not increase NMIIA accumulation at apical junctions (Fig. 8B,B′,H) as seen in wild-type Flag-Lmo7 (Fig. 8C,C′,G). Importantly, neither GFP-Lmo7(AAAA) nor GFP-Lmo7(AAAK) induced apical constriction in ectodermal cells (Fig. S4B-E). These results indicate that Lmo7 binding to NMII via NMIIBD is required for Lmo7-mediated apical constriction.

Although necessary, Lmo7 binding to NMII was not sufficient for apical constriction. Although Lmo7(aa 242-400) bound to NMIIA (Fig. 7A), its overexpression did not stimulate NMIIA accumulation at apical junctions (Fig. S5G,H) or induce apical constriction (Fig. 6). By contrast, Lmo7(aa 242-709) that contains an α-actinin-binding region was still able to stimulate NMIIA accumulation (Fig. 8D-F″,I) and triggered apical constriction (Fig. 6). Lmo7(aa 242-400) and Lmo7(aa 242-709) showed similar levels of accumulation at apical junctions (Fig. 5A-F″), suggesting that loss of apical constriction by Lmo7(aa 242-400) is not due to reduced localization at apical junctions. Notably, although full-length Lmo7 promoted the formation of thick and dense F-actin networks (Fig. 4), Lmo7(aa 242-709) did not exhibit these effects (Fig. S5I,J). These results suggest that NMII is a primary cellular target of Lmo7 in apical constriction, although other proteins, such as α-actinin, are involved.

The role of Lmo7 in NMII localization has been further confirmed in loss-of-function experiments. We observed reduced GFP-NMIIA localization at apical junctions in the cells depleted of

Development (2022) 149, dev200236. doi:10.1242/dev.200236

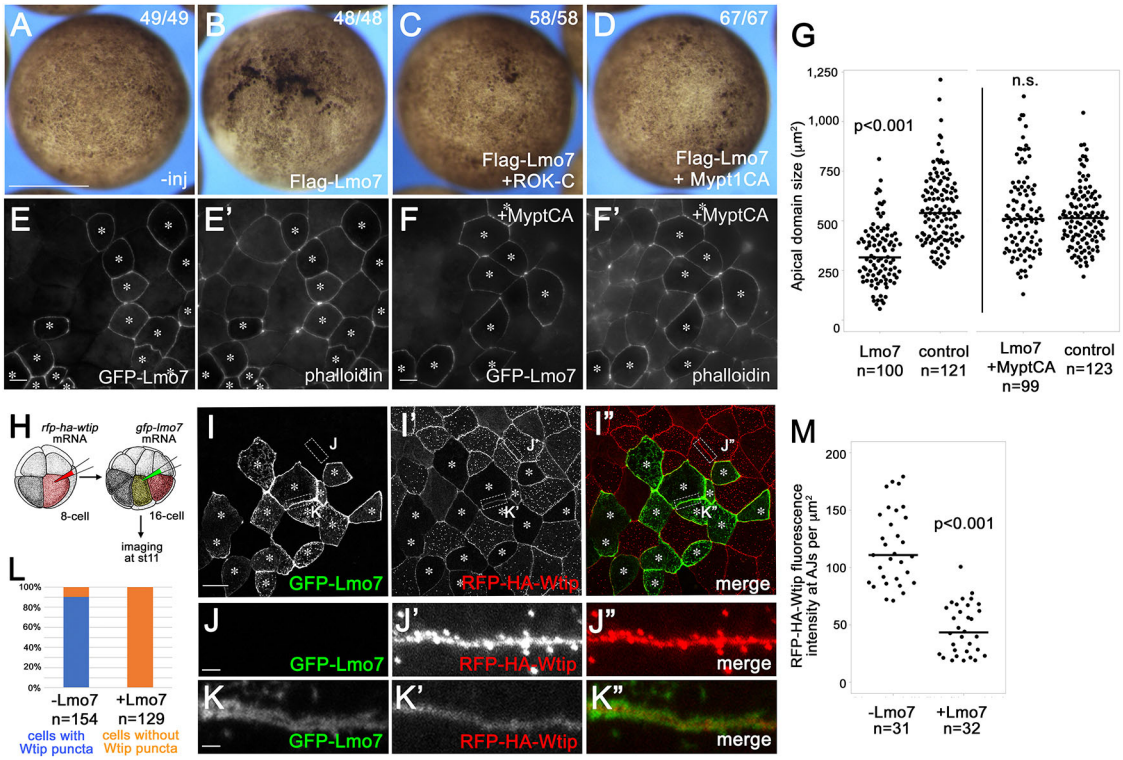

Fig. 5. Effects of Lmo7 on actomyosin contractility require the Rho-ROCK-NMII pathway. (A-D) Pigment granule accumulation at stage 11. Two blastomeres of four- to eight-cell stage embryos were injected with relevant RNA. (A) Control uninjected and (B) Flag-Lmo7-treated (500 pg RNA) embryos. (C) Embryos injected with Flag-Lmo7 (500 pg RNA) and ROK-C (200 pg RNA), and (D) embryos injected with Flag-Lmo7 (500 pg RNA) and Mypt1CA (50 pg RNA). Images are representative of three experiments. (E-F′) The *en face* view of the ectodermal cells expressing GFP-Lmo7 alone (200 pg RNA) (E,E′) or together with MyptCA (50 pg RNA) (F,F′). Asterisks indicate cells expressing relevant proteins. (G) Quantification of the apical surface area related to images in E-F″. Individual data points are included with the median indicated by a horizontal line. (H-M) Lmo7 modulates RFP-HA-Wtip localization. (H) Experimental design. Embryos were sequentially injected into a ventral blastomere with RFP-HA-Wtip RNA (200 pg) (in red, four- to eight-cell stage) and GFP-Lmo7 RNA (500 pg) (in yellow, 16- to 32-cell stage), causing protein co-expression in 25-50% cells at stage 11 (asterisks in I-I″). (I-I″) RFP-HA-Wtip puncta localization in cells with or without GFP-Lmo7. Areas in I-I″ are enlarged in J-K″. RFP-HA-Wtip forms puncta near apical junctions and the apical cortex in the absence of Lmo7. (J-K″) Effects of Lmo7 on RFP-HA-Wtip puncta formation near apical junctions. RFP-HA-Wtip forms a smooth line between the Flag-Lmo7 double bands (K-K″). (L) Quantification of the Lmo7 effect on RFP-HA-Wtip puncta formation near the apical cortex. Cells with and without apical Wtip puncta were counted in the control (–Lmo7, *n*=154) and Lmo7-expressing cells (+Lmo7, *n*=129). (M) Quantification of the Lmo7 effect on RFP-HA-Wtip puncta near apical junctions. Fluorescence intensity of RFP-HA-Wtip near apical junctions was measured. Scale bars: 500 µm in A; 10 µm in E and I; 2 µm in J and K. Statistical significance of the difference was assessed by the Mann–Whitney U-test.

Lmo7 (Fig. 9A-C). Nevertheless, the Lmo7-depleted cells preserved normal morphology with unaltered distribution of ZO-1 (Fig. 9D,E). F-actin accumulation at apical junctions was not altered either (Fig. 9F,G). Taken together, our findings suggest that Lmo7 functions to maintain NMII at apical junctions.

Neural tube closure is delayed in Lmo7 knocked-down embryos

To evaluate Lmo7 function during different developmental processes, we first examined the temporal and spatial expression of *Lmo7* transcripts in *Xenopus* embryos. RT-PCR analysis demonstrated ubiquitous presence of *Lmo7* transcripts at different stages of embryonic development, including the maternal expression (Fig. S6A). *In situ* hybridization analysis revealed broad expression of *Lmo7* in epidermal ectoderm and neuroectoderm (Fig. S6B-E). Of note, Lmo7 transcripts showed a ‘salt-and-pepper’ pattern in late gastrula dorsal ectoderm (Fig. S6B). In the late neurula, Lmo7 was detectable at high levels in preplacodal ectoderm (Fig. S6H,I), somitic mesoderm (Fig. S6I,J) and the surface neuroepithelial layer (Fig. S6F,G). In tailbud and more advanced embryos, *Lmo7* RNA was detected in the skin and pharyngeal arches (Fig. S6K-O). *Lmo7* was also expressed in the somites (Fig. S6K,L,N) and the heart (Fig. S6M), consistent with previously proposed role of Lmo7 in muscle development (Holaska et al., 2006; Lao et al., 2015; Mull et al., 2015).

Neuroectodermal expression of Lmo7 and its ability to induce apical constriction suggested a possible role of *Lmo7* in neural tube closure. A translation blocking morpholino (MO) was injected into one side of embryos at 2- to 4-cell stage, together with *gfp* RNA to label the injected side. The morphants exhibited incomplete neural tube closure in stage 20 embryos (compare Fig. 9H and I; black arrow in Fig. 9I, Movie 1), indicating inefficient apical constriction. This modest defect in neural tube closure was quantified by measuring the width of neural tube opening in embryos injected with *Lmo7* translation- or splicing-blocking MOs (Fig. 9J-L, Fig. S7C). Taken together, these results demonstrate the requirement of Lmo7 for neural tube closure in *Xenopus* embryos.

DISCUSSION

In this study, we identify Lmo7 as a novel regulator of actomyosin contractility and apical domain size in *Xenopus* embryonic ectoderm. Lmo7 localizes to actomyosin networks at apical junctions and the apical cortex. Embryonic cells expressing Lmo7 form thicker and denser actomyosin network when compared with

Development (2022) 149, dev200236. doi:10.1242/dev.200236

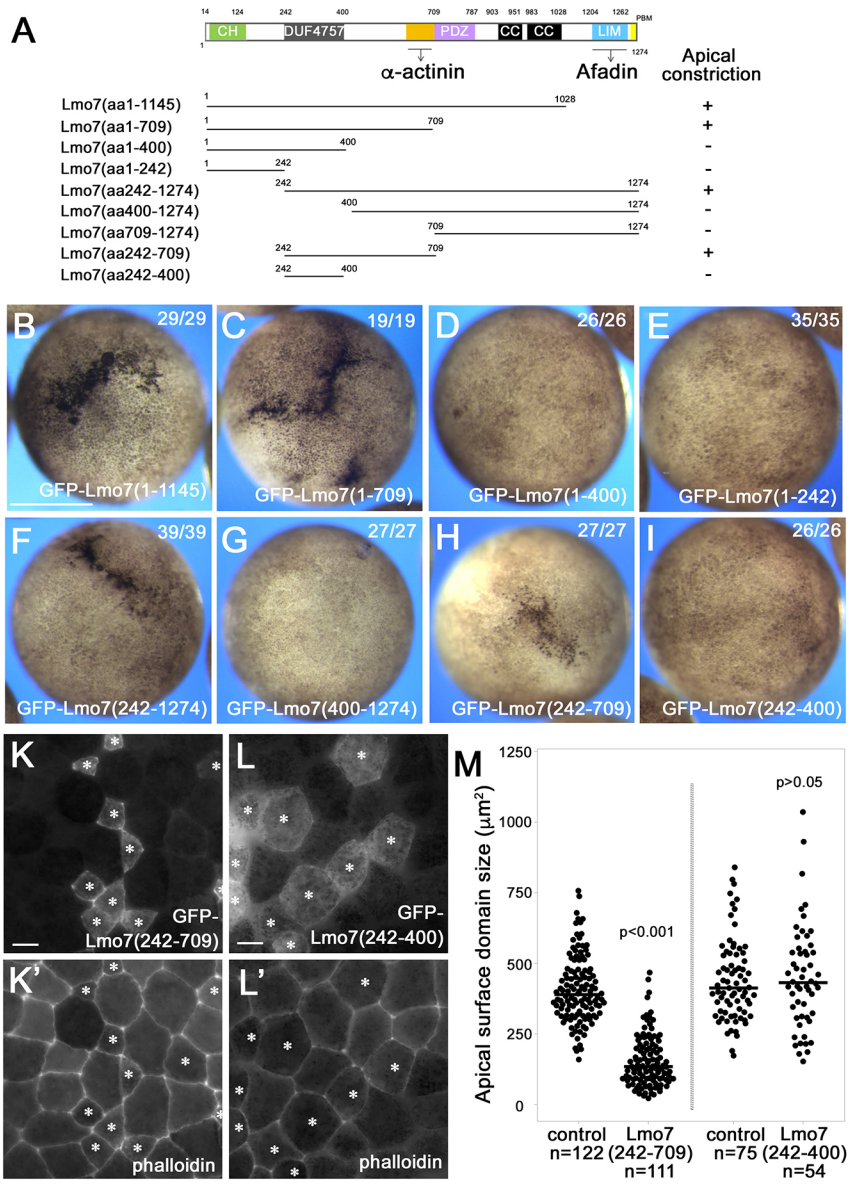

Fig. 6. Identification of Lmo7 domains required for apical constriction. (A) Structure of Lmo7 and the mutants used in this study. Lmo7 has the N-terminal calponin homology (CH) domain, DUF4757, the α-actinin binding region, the PDZ domain, two coiled-coil domains and the C-terminal LIM domain. (B-I) Representative images of stage 11 embryos injected with RNA encoding various Lmo7 constructs (1 ng). Apical constriction was assessed by pigment granule accumulation. Apical constriction induced by Lmo7 constructs lacking the LIM domain (B), and the coiled-coil and PDZ domains (C). Deletion of the α-actinin-binding region (D) and DUF4757 (E) eliminates the activity of pigment granule accumulation, whereas CH domain deletion has no visible effect (F). Lmo7(aa 400-1274) lacking DUF4757 has no pigment granule accumulation activity (G). The region containing the DUF4757 domain and α-actinin-binding region Lmo7(aa 242-709) was the shortest fragment that induced pigment granule accumulation (H). The DUF4757 domain has no effect on its own (I). (K-L′) Effects of GFP-Lmo7(aa 242-709) and GFP-Lmo7(aa 242-400) on apical domain size. GFP-Lmo7 deletion mutants were mosaically expressed by RNA injection (500 pg, asterisks) in four- to eight-cell stage embryos. GFP fluorescence and phalloidin staining are shown in stage 11 ectoderm. (M) Quantification of apical surface domain size related to K-L′. Apical domain surface size of control cells was measured only in cells that shared at least one cell boundary with cells expressing GFP-Lmo7 mutants. Images for scoring were taken from at least five embryos. Data are representative of more than three independent experiments. Individual data points are included with the median indicated by a horizontal line. Scale bars: 500 µm in B-I; 10 µm in K,L. Statistical significance of the difference was assessed by the Mann–Whitney U-test.

control ectoderm. We find that Lmo7 binds NMII heavy chains via NMIIBD, a domain with previously unknown function, and observe a tight correlation between apical constriction inducing activity of Lmo7 deletion mutants and NMII recruitment to the cell cortex. We propose that Lmo7 triggers apical constriction by promoting NMII incorporation into actomyosin networks.

The striking localization of Lmo7 to two cortical bands on both sides of the apical cell-cell junction is similar to the distribution of NMIIA in the normal tissue, including non-sensory epithelial cells of the mammalian inner ear (Ebrahim et al., 2013). In gain-of-function experiments, Lmo7 promoted the formation of organized peri-junctional actomyosin bundles. Our knockdown experiments revealed expanded apical domain in ectoderm cells and reduced NMIIA at apical junctions. These observations suggest that Lmo7 triggers apical constriction via a 'purse-string' mechanism. Similar actomyosin enrichment with 'sarcomere-like' organization of NMII was described in MDCK cells depleted of ZO proteins, suggesting a crosstalk between apical junctions and actomyosin (Choi et al., 2016; Fanning et al., 2012; Tokuda et al., 2014; Van Itallie et al., 2009; Yu-Kemp et al., 2022). In contrast to ZO protein, which may be inhibitory, Lmo7 appears to promote the sarcomere-like organization.

The ability of Lmo7 to promote peri-junctional actomyosin bundles does not exclude a role for Lmo7 in the medioapical actomyosin network. The importance of medioapical actomyosin for apical constriction has been intensively studied in *Drosophila* and other invertebrates (An et al., 2017; Azevedo et al., 2011; Blanchard et al., 2010; David et al., 2010; Martin et al., 2009; Mason et al., 2013; Royou et al., 2002). We found increased junctional and medioapical F-actin and NMIIA in Lmo7-expressing cells. These observations lead us to propose that Lmo7 is responsible for the organization and contractility of apical actomyosin networks. Further studies will be necessary to understand how circumferential actomyosin and medioapical actomyosin cooperate to induce apical constriction in vertebrate epithelia and how Lmo7 involves in this process.

Compared with strong effects of Lmo7 overexpression in actomyosin reorganization, *Lmo7* knockdown in *Xenopus* embryos showed relatively mild defects. The observed effects on normal ectoderm are consistent with a general function of Lmo7 in actomyosin network architecture and apical domain regulation,

Development (2022) 149, dev200236. doi:10.1242/dev.200236

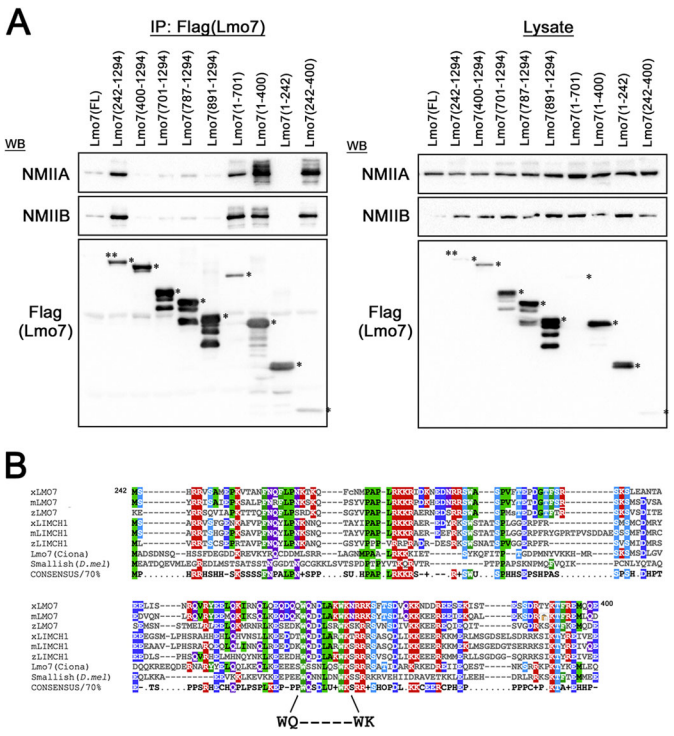

Fig. 7. The DUF4757 domain binds to NMII heavy chain. (A) NMIIA and NMIIB co-precipitate with Flag-Lmo7 in HEK293 T cells. Asterisks indicate protein bands corresponding to full-length or deletion mutant forms of Lmo7. Lmo7(aa 242-400) containing DUF4757 is sufficient to co-precipitate endogenous NMIIA and NMIIB. (B) The alignment of DUF4757/NMIIBD sequences. *Xenopus laevis* Lmo7 (NM_001135230), *Mus musculus* Lmo7 (XM_006519190), *Danio rerio* Lmo7 (XM_021478660), *Xenopus laevis* LIMCH1 (NM_001096206), *Mus musculus* LIMCH1 (NM_001001980), *Danio rerio* LIMCH1 (XM_009291008), *Ciona intestinalis* Lmo7 (XM_002128910) and *Drosophila melanogaster* Smallish (NM_169014). Conserved positively charged, negatively charged, hydrophobic or hydrophilic amino acids are marked by red, blue, green and purple, respectively. Ser or Thr residues are marked by light blue. Consensus sequence based on amino acid similarity (>70%) is shown at the bottom. The conserved WQ-WK sequence used for AA-AA substitution is indicated.

rather than exclusively in apical constriction. Nevertheless, in agreement with the role in apical constriction, Lmo7 morphants exhibited a delay in neural tube closure. The neural tube defects were relatively mild, suggesting that the loss of Lmo7 is functionally compensated for by other proteins, such as its paralogue Limch1 (Lin et al., 2017). *Lmo7* knockout mice also exhibit limited developmental defects in specific epithelia (Du et al., 2019; Lao et al., 2015; Tanaka-Okamoto et al., 2009), indicating similar compensation mechanisms in higher vertebrates. On the other hand, *Drosophila* embryos lacking Smallish, the fly orthologue of Lmo7, are defective in epithelial morphogenesis (Beati et al., 2018), pointing to the indispensable role of Smallish in actomyosin control. Double knockout of *Lmo7* and *Limch1* is necessary to properly evaluate their loss-of-function phenotypes in vertebrates.

Our experiments show that the ability of Lmo7 to trigger apical constriction depends on the recruitment of NMII heavy chains. It remains unclear how Lmo7 increases the actomyosin contractions after NMII recruitment. Lmo7 may recruit or activate Rho or ROCK to increase MRLC phosphorylation. Alternatively, Lmo7 may stimulate ATPase activity of the NMII head motor domain, or increase NMII heavy chain phosphorylation (Conti et al., 1991; Dulyaninova et al., 2007; Even-Faitelson and Ravid, 2006; Murakami et al., 1998) or NMII interaction with other proteins (Dahan et al., 2012; Dulyaninova et al., 2005; Elliott et al., 2012; Garrett et al., 2006). Of note, NMIIBD is disrupted in certain splicing variants of Lmo7 (Fig. S8) and only the second half of it is conserved in *Drosophila* Smallish (Fig. 7B). In addition to recruiting NMII to apical junctions, Lmo7 might act as a scaffold to position F-actin, NMII and α-actinin in the circumferential actomyosin bundles, and organize them in a sarcomere-like pattern. The domains that may interact with F-actin are the CH domain and the afadin-binding LIM domain (Ooshio et al., 2004). Surprisingly, Lmo7(aa 242-709) lacking both the CH and LIM domains retained the ability to trigger apical constriction but did not cause any further visible F-actin enrichment. Because Lmo7(aa 242-709) contains domains that bind NMII and α-actinin, Lmo7(aa 242-709) may work as a linker to stabilize NMII and α-actinin in apical actomyosin networks. This would be consistent with the 'ratchet' model of apical constriction that includes repeated cycles of actomyosin contraction and stabilization (Martin et al., 2009). Further studies are needed to understand how Lmo7 promotes F-actin enrichment or polymerization in the apical domain of cells, and how Lmo7(aa 242-709) promotes apical constriction without such F-actin enrichment.

The effect of Lmo7 on actomyosin network is likely relevant to mechanotransduction processes at apical junctions. Lmo7 levels increase in response to the mechanical force (Hashimoto et al., 2019). Lmo7 binds afadin, which has been implicated in force transmission at cell-cell junctions (Choi et al., 2016; Manning et al., 2019; Yu and Zallen, 2020). Supporting this hypothesis, we found that Lmo7 influences the distribution of Wtip, a sensor of mechanical tension (Chu et al., 2018). The remaining challenge is to determine how the interplay of Lmo7, afadin and other junctional proteins leads to effective generation, sensing and transmission of mechanical forces during epithelial morphogenesis.

MATERIALS AND METHODS

Plasmids

Xenopus laevis Lmo7 cDNA clone was obtained from Dharmacon. Full-length and truncated forms of Lmo7 were PCR amplified and cloned into a pCS107-Flag, -HA or -GFP expression vector using standard protocols. Primers used for the amplification are in Table S1. pCS2-RFP-HA-Wtip has been previously described (Chu et al., 2018). pCS2-GFP-NMIIA and pCS2-GFP-NMIIB were subcloned from CMV-GFP-NMHC II-A and CMV-GFP-NMHC II-B (Addgene 11347 and 11348)(Wei and Adelstein, 2000). pCS2-GFP-α-actinin 4 was constructed from pCS2-hiActTS-GR (a gift from Tatsuo Michiue, The University of Tokyo, Japan). pCS2-ROK-C and pCS2-Mypt1CA were from Florence Marlow (Icahn School of Medicine at Mount Sinai, New York, USA; Marlow et al., 2002) and David Kimelman (The University of Washington, Seattle, WA, USA; Weiser et al., 2009), respectively.

Xenopus embryo culture and microinjections of RNA and morpholinos

Wild-type *Xenopus laevis* adults were purchased from Nasco, and maintained and handled according to the recommendations in the Guide for the Care and Use of Laboratory Animals of the National Institutes of Health. A protocol for animal use was approved by the Institutional Animal Care and Use Committee (IACUC) at Icahn School of Medicine at Mount Sinai. *In vitro* fertilization and embryo culture were performed as described previously (Dollar et al., 2005). Embryo staging was determined according to Nieuwkoop and Faber (1967). For microinjections, embryos were transferred into 3% Ficoll 400 (Pharmacia) in 0.5× Marc's modified Ringer's (MMR) solution [50 mM NaCl, 1 mM KCl, 1 mM CaCl2, 0.5 mM MgCl2 and 2.5 mM HEPES (pH 7.4)] (Peng, 1991). Linearized plasmid DNA was used to synthesize capped RNA using mMessage mMachine

Development (2022) 149, dev200236. doi:10.1242/dev.200236

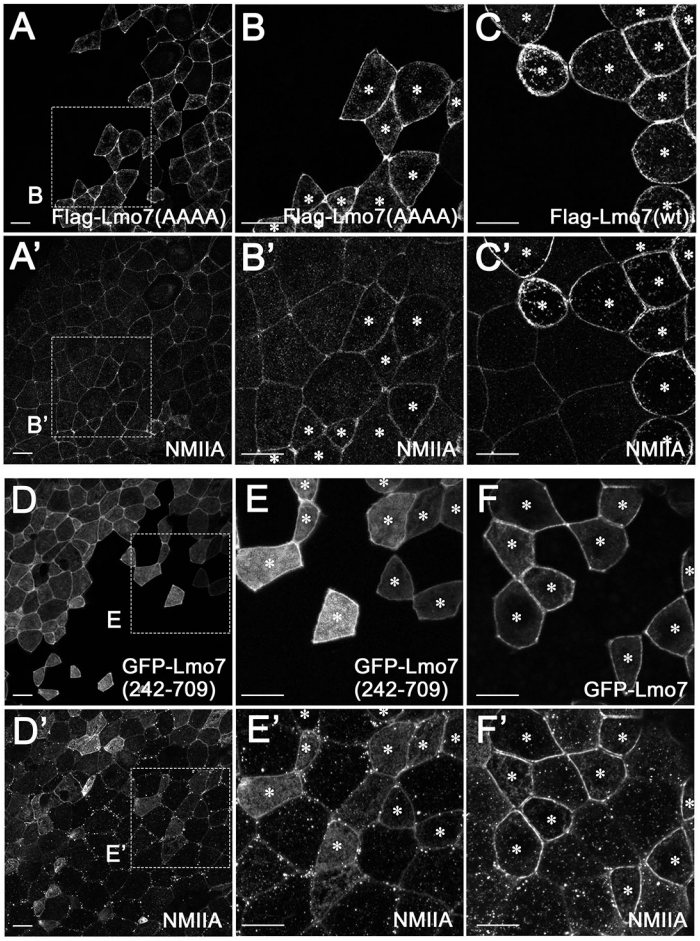

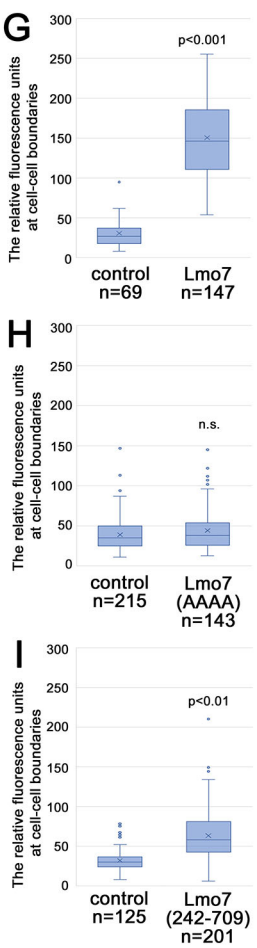

Fig. 8. Lmo7 recruits NMII to apical junctions through NMIIBD. Embryos at the four- to eight-cell stage were injected with RNAs (0.5-1 ng) encoding full-length or mutant forms of Lmo7. The superficial ectoderm was imaged at stage 11 after staining using anti-Flag, GFP or NMIIA antibodies. Cells expressing Flag-Lmo7 constructs are marked by asterisks. (A-B′) Lmo7(AAAA) does not cause NMIIA enrichment at apical junctions. Areas marked by rectangles in A and A′ are enlarged in B and B′. (C,C′) NMIIA enrichment in embryo expressing Flag-Lmo7, for comparison purposes. (D-E′) Lmo7(aa 242-709) increases NMIIA accumulation. Areas marked by rectangles in D and D′ are enlarged in E and E′. (F,F′) NMIIA enrichment in embryo expressing GFP-Lmo7, for comparison purposes. (G-I) Quantification of NMIIA accumulation at apical junctions in cells expressing GFP-Lmo7 (G), Flag-Lmo7(AAAA) (H) or GFP-Lmo7(aa 242-709) (I). Fluorescence intensity of NMIIA was measured at 3-10 locations within individual cell-cell boundaries. GFP-Lmo7(242-709) recruits NMIIA less effectively than full-length Lmo7. Boxes and whiskers indicate the lower and upper quartiles, and variabilities outside the upper and lower quartiles. Statistical significance of the difference was assessed by the Mann–Whitney U-test. Scale bars: 10 µm.

SP6 Transcription kit (Invitrogen). Synthesized RNA was purified by LiCl precipitation. RNA in 5-10 nl of RNase-free water (Invitrogen) was microinjected into one or two blastomeres of four- to 16-cell stage embryos. Morpholino oligonucleotide (MO) specific for Lmo7 was purchased from Gene Tools, and had the following sequence: *Lmo7*-ATGMO, 5′-GAATTTTCATTCCATTCCATTG-3′; *Lmo7*-spMO, 5′-AAATGCAAAGAATGTACTTACTCGC-3′. GFP or memGFP RNA was co-injected with MO for lineage tracing. Imaging of GFP-negative cells was carried out at least 20 cells away from the boundary region, to take account of the difference in diffusion of RNA and MO.

Cell culture and transfection

HEK293T cells were purchased from ATCC and maintained in Dulbecco's modified eagle media (DMEM) (Corning) supplemented with 10% fetal bovine serum (Sigma) in a 37°C incubator with 5% CO_2. HEK293T cells grown in 60 mm dishes to 70-80% density were transfected with a mixture of 4 µg plasmid DNA and 20 µg polyethylenimine (Polysciences). Cell lysates were extracted 24 h after transfection.

Immunoprecipitation and immunoblotting

Cell lysates were extracted from HEK293T cells using RIPA buffer [50 mM Tris-HCl (pH 7.4), 150 mM NaCl, 1% NP-40, 0.5% sodium deoxycholate and 0.1% SDS] supplemented with Protease Inhibitor Cocktail III (Calbiochem) and PhosStop phosphatase inhibitor cocktail (Roche). Cell lysates were incubated with anti-Flag M2 agarose (Sigma) at 4°C for at least 6 h. Agarose beads were washed three times in Tris-buffered saline containing 0.05% Triton X-100 (TBST). Agarose beads were heated at 95°C for 5 min in SDS sample buffer containing 5% β-mercaptoethanol (Sigma). After SDS-PAGE and transfer to a nitrocellulose membrane with a 0.2 µm pore size (BioRad), immunoblotting was carried out with the following antibodies: rabbit anti-NMIIA pAb (BioLegend, POLY19098, 1:500), rabbit anti-NMIIB pAb (BioLegend, POLY19099, 1:500), mouse anti-DYKDDDDK mAb clone 2H8 (Cosmo Bio, KAL-K0602, 1:1000) and mouse anti-GFP mAb clone B2 (Santa Cruz Biotechnology, sc-9996, 1:500). HRP-conjugated secondary antibodies against mouse or rabbit IgG were from Cell Signaling Technology (7074 and 7076, 1:5000). Chemiluminescent signals were acquired using Clarity ECL Western Blotting Substrates (BioRad) on the ChemiDoc MP Imaging System (BioRad).

Xenopus embryo lysates were made by incubating 20 embryos in 400 µl lysis buffer [50 mM Tris-HCl (pH 7.6), 50 mM NaCl, 1 mM EDTA and 1% Triton X-100] supplemented with protease inhibitor and protein phosphatase inhibitor cocktails as described above. After centrifugation for 3 min at 16,000 ***g***, the supernatant was mixed with SDS-sample buffer, followed by standard SDS-PAGE and western blot protocol. Experiments were repeated at least three times.

In situ hybridization

Digoxigenin-11-UTP-labeled *Lmo7L* RNA probes, sense and antisense, were prepared from linearized plasmids containing *Xenopus Lmo7 L* cDNA, using SP6 or T7 RNA polymerase (Promega) and DIG RNA labeling kit (Roche). Three independent probes were used to confirm the specificity of *Lmo7 L* expression. *In situ* hybridization was conducted following a standard protocol described by Harland (1991), with some modifications. After hybridization, embryos were incubated with anti-digoxigen-AP antibody (Roche). BCIP/NBT Alkaline phosphatase substrate kit (Vector laboratory) was used for color reaction. Embryo images were captured using a Leica stereo-microscope equipped with a color CCD camera.

Analysis of pigment granule accumulation

Capped RNAs encoding Lmo7, Lmo7 mutants, ROK-C or Mypt1-CA were injected into two animal-ventral blastomeres of four-cell embryos. For analysis of pigment granule accumulation, embryo images were captured

Development (2022) 149, dev200236. doi:10.1242/dev.200236

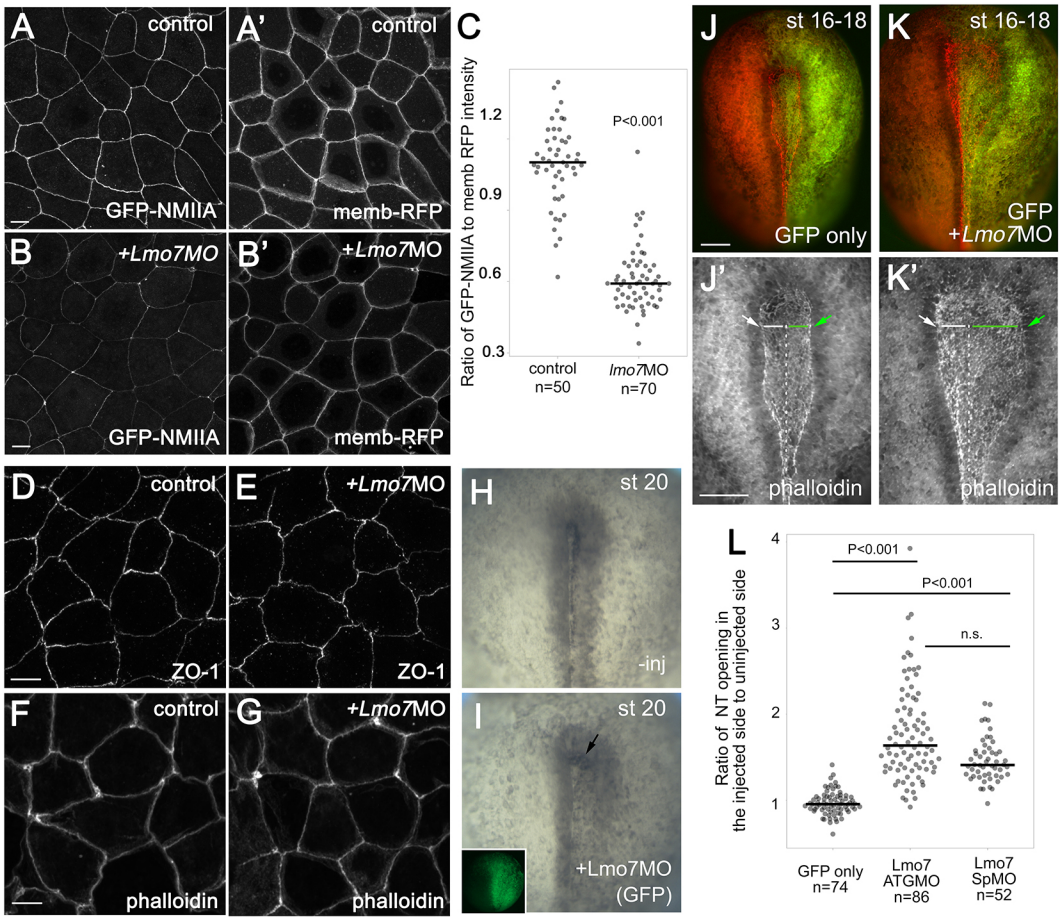

Fig. 9. Lmo7 knockdown reduces NMIIA at apical junctions and delays neural tube closure. (A-E′) RNAs encoding GFP-NMIIA (200 pg) and membrane-tethered RFP (100 pg) were co-injected into one ventral blastomere of four- to eight-cell stage embryos, with or without *Lmo7* ATGMO (30 ng). At stage 11, embryos were stained using phalloidin or anti-ZO-1 antibodies. (A-B′) Reduced GFP-NMIIA enrichment at apical junctions in *lmo7*MO embryos. (C) Quantification of GFP-NMIIA enrichment at apical junctions in control cells (*n*=50) and Lmo7MO cells (*n*=70). GFP-NMIIA fluorescence intensity was normalized by memb-RFP fluorescence in individual cell-cell boundaries. Individual data points are included with the median indicated by a horizontal line. (D-G) Endogenous ZO-1 and F-actin distribution did not significantly change in control (D,F) and *lmo7* MO embryos (E,G). (H-L) Effects of Lmo7 knockdown on neural tube closure. Lmo7 ATGMO (30 ng) or Lmo7 splice-blocking morpholino (spMO, 10 ng) (Fig. S7A,B) was co-injected with GFP RNA (50 pg, lineage tracer) into the right side of two- to four-cell stage embryos. (H,I) The bright-field images of an uninjected embryo and an embryo injected with Lmo7ATGMO at stage 20. The most anterior part of the neural tube remains open in the MO-injected side (arrow in I). Time-lapse imaging is shown in Movie 1. (J-K′) Representative images of embryos injected with GFP RNA alone (J,J′) or with Lmo7ATG MO (K,K′). Dorsal view. Stage 16-18 embryos were co-stained with phalloidin. White dotted lines represent the midline. (L) Quantification of neural tube closure related to images in J-K′. The ratio of neural tube opening on the injected versus uninjected side is shown. Neural tube opening was assessed by the widest distance from the midline (white dotted lines in J′ and K′) to the fusing edge of the neural fold [shown by white (–injection) or green (+injection) arrows in J′,K′]. The original data measuring neural tube opening in individual embryos is shown in Fig. S7C. Statistical significance of the difference between the median values was assessed by the Dunn's test using a Bonferroni correction for the *P*-values. Scale bars: 10 µm.

using a Leica stereo microscope equipped with a color CCD camera. Each experiment included 20-30 embryos per condition. Experiments were repeated at least three times.

Whole-mount immunocytochemistry

For formaldehyde fixation, *Xenopus* embryos were devitellinized manually using forceps and fixed in MEMFA [0.1 M MOPS (pH 7.4), 2 mM EGTA, 1 mM MgSO4 and 3.7% formaldehyde] (Harland, 1991) for 60 min at room temperature. After washing in phosphate-buffered saline (PBS), embryos were permeabilized in 0.1% Triton in PBS for 30 min. For trichloroacetic acid (TCA) fixation, devitellinized embryos were fixed in ice-cold 10% TCA for 30 min. Embryos were then incubated in 1% BSA in TBS at 4°C overnight for blocking. After that, embryos were incubated with primary antibodies in 1% BSA, 1% DMSO in PBS or TBS at 4°C overnight. Antibodies used in this study are the following: rabbit anti-NMIIA pAb (BioLegend, POLY19098, 1:300), rabbit anti-Myosin light chain (phospho S20) pAb (Abcam, ab2480, 1:500), mouse anti-DYKDDDDK mAb clone 2H8 (Cosmo Bio, KAL-K0602, 1:500), rat anti-HA mAb clone 3F10 (Roche, 118673230002, 1:100), mouse anti-ZO1 mAb clone T8-754 (Itoh et al., 1993), rabbit anti-β-catenin pAb (Santa Cruz Biotechnology, sc-7199, 1:500) and chicken anti-GFP pAb (Abcam, ab13970, 1:500). After washing in PBS or TBS three times, embryos were incubated with secondary antibodies conjugated with either Alexa 488, Cy3 or Cy2 fluorescent dyes in 1% BSA and 1% DMSO in PBS at 4°C overnight. Alexa 488-, Cy3- or Cy2-conjugated secondary antibodies against mouse, rat and rabbit IgG or chicken IgY were obtained from Invitrogen (A-32723 and A-11034, 1:300) or Jackson ImmunoResearch Laboratory (711-165-152, 715-165-151, 712-165-153 and 703-225-155, 1:500). AlexaFluor 555-phalloidin (Invitrogen, A34055) was added to the secondary antibody solution to label F-actin. After washing in PBS or TBS three times, embryos were transferred in 25% glycerol in PBS. The animal pole side of embryos was dissected manually by forceps and mounted on slide glasses using Vectashield mounting medium (Vector). Imaging was carried out using Zeiss AxioImager upright microscope with Zeiss Axiocam CCD camera or Zeiss LSM880 confocal

microscope system. Images were captured from at least five independent embryos. Experiments were repeated at least three times. Captured images were processed and quantified using ImageJ software.

Time-lapse imaging of *Xenopus* embryos

Lmo7 ATGMO (30 ng) was injected into two right blastomeres of four-cell stage embryos, with GFP RNA (100 pg) as a tracer. The vitelline membrane was manually removed using forceps at stage 15. An embryo was placed into a small hole on 1% agarose gel in 0.1×MMR to stabilize its position. Time-lapse imaging was carried out using the AxioZoomV16 fluorescence stereomicroscope (Zeiss) equipped with the AxioCam 506 mono CCD camera (Zeiss).

Quantification and statistical analyses

To quantify apical domain size, embryos injected with relevant RNA or MOs were co-stained with Alexa Fluor 555-conjugated phalloidin (ThermoFisher Scientific). To measure the apical domain surface area, animal pole ectoderm samples were flat-mounted *en face* on glass slides. After image acquisition, the apical domains of individual cells were manually outlined using a free-hand line tool in ImageJ based on phalloidin staining, and the area of the apical domain was measured using ImageJ. For Lmo7 cells, only cells that shared at least one boundary with control wild-type cells were used for quantification. For control cells, only cells that shared at least one boundary with Lmo7 cells were used.

To quantify the ratio of apical width to basolateral length, gelatin-embedded embryos stained with Alexa Fluor 555-conjugated phalloidin (ThermoFisher Scientific, A34055, 1:200) were cryosectioned as described previously (Ossipova and Sokol, 2021) using MEMFA as a fixative. After image acquisition, the apical membrane and the basolateral membrane of individual cells were manually outlined on cross-sections based on phalloidin staining. Their length was measured using ImageJ.

To quantify the enrichment of Lmo7, F-actin and endogenous NMIIA at apical junctions, five to ten circles ∼2 µm in diameter were randomly drawn in cell-cell boundaries. Only cell-cell boundaries formed between two Lmo7-expressing cells or two control cells were selected. Tricellular vertices were excluded for simplicity. To quantify medioapical enrichment of Lmo7, F-actin and NMIIA, a 10 µm circle was drawn in the center of individual cells. ImageJ was used to measure the integrated fluorescence intensity within the selected area.

To quantify the junctional enrichment of exogenously expressed GFP-NMIIA in *Lmo7* morphants, individual cell-cell boundaries were marked with a 2 µm wide line, using a free-hand line tool in ImageJ. Tricellular vertices were excluded. The fluorescence intensity of GFP-NMIIA in these lines were measured and normalized to that of membrane-tethered RFP. To quantify Wtip puncta formation near apical junctions, cell-cell boundaries formed between Lmo7- and Wtip-expressing cells or between the cells expressing only Wtip (control cells) were selected. The fluorescence intensity of RFP-HA-Wtip per μm^2 was measured using ImageJ.

For statistical analysis, the Mann–Whitney U-test was used to determine the statistical significance between two groups. Statistical significance of the difference among more than three groups was assessed by Dunn's test using a Bonferroni correction for the *P*-values.

Neural tube opening was assessed in embryos at stage 16-18. A series of *z*-stack images was captured on the AxioZoomV16 fluorescence stereomicroscope (Zeiss) equipped with the AxioCam 506 mono CCD camera (Zeiss). Individual *z*-stage images were processed into a single image using the 'extended depth of focus' module on the Zeiss Zen (blue edition) imaging software. The widest distance from the midline to the fusing edge of the neural fold was measured using ImageJ.

Acknowledgements

We thank Robert Adelstein, Florence Marlow, Tatsuo Michiue and David Kimelman for plasmids, Pamela Mancini for help with Lmo7 mutagenesis at the early stages of this project, and members of the Sokol laboratory for discussions. We acknowledge the help from the ISMMS Microscopy Core facility.

Competing interests

The authors declare no competing or financial interests.

Author contributions

Conceptualization: M.M., S.Y.S.; Methodology: M.M., S.Y.S.; Validation: M.M.; Formal analysis: M.M.; Investigation: M.M., C.-W.C.; Resources: S.Y.S.; Writing - original draft: M.M.; Writing - review & editing: M.M., S.Y.S., C.-W.C.; Visualization: M.M.; Funding acquisition: S.Y.S.

Funding

This work was supported by the National Institutes of Health (R35GM122492 to S.Y.S.). Deposited in PMC for release after 12 months.

Peer review history

The peer review history is available online at https://journals.biologists.com/dev/article-lookup/doi/10.1242/dev.200236

References

Abe, K. and Takeichi, M. (2008). EPLIN mediates linkage of the cadherin catenin complex to F-actin and stabilizes the circumferential actin belt. *Proc. Natl. Acad. Sci. USA* **105**, 13-19. doi:10.1073/pnas.0710504105

Agarwal, P. and Zaidel-Bar, R. (2019). Principles of actomyosin regulation In Vivo. *Trends Cell Biol.* **29**, 150-163. doi:10.1016/j.tcb.2018.09.006

An, Y., Xue, G., Shaobo, Y., Mingxi, D., Zhou, X., Yu, W., Ishibashi, T., Zhang, L. and Yan, Y. (2017). Apical constriction is driven by a pulsatile apical myosin network in delaminating Drosophila neuroblasts. *Development* **144**, 2153-2164.

Arnold, T. R., Shawky, J. H., Stephenson, R. E., Dinshaw, K. M., Higashi, T., Huq, F., Davidson, L. A. and Miller, A. L. (2019). Anillin regulates epithelial cell mechanics by structuring the medial-apical actomyosin network. *Elife* **8**, e39065.

Azevedo, D., Antunes, M., Prag, S., Ma, X., Hacker, U., Brodland, G. W., Hutson, M. S., Solon, J. and Jacinto, A. (2011). DRhoGEF2 regulates cellular tension and cell pulsations in the Amnioserosa during Drosophila dorsal closure. *PLoS One* **6**, e23964. doi:10.1371/journal.pone.0023964

Balashova, O. A., Visina, O. and Borodinsky, L. N. (2017). Folate receptor 1 is necessary for neural plate cell apical constriction during Xenopus neural tube formation. *Development* **144**, 1518-1530.

Beati, H., Peek, I., Hordowska, P., Honemann-Capito, M., Glashauser, J., Renschler, F. A., Kakanj, P., Ramrath, A., Leptin, M., Luschnig, S. et al. (2018). The adherens junction-associated LIM domain protein Smallish regulates epithelial morphogenesis. *J. Cell Biol.* **217**, 1079-1095. doi:10.1083/jcb.201610098

Blanchard, G. B., Murugesu, S., Adams, R. J., Martinez-Arias, A. and Gorfinkiel, N. (2010). Cytoskeletal dynamics and supracellular organisation of cell shape fluctuations during dorsal closure. *Development* **137**, 2743-2752. doi:10.1242/dev.045872

Boller, K., Vestweber, D. and Kemler, R. (1985). Cell-adhesion molecule uvomorulin is localized in the intermediate junctions of adult intestinal epithelial cells. *J. Cell Biol.* **100**, 327-332. doi:10.1083/jcb.100.1.327

Bresnick, A. R. (1999). Molecular mechanisms of nonmuscle myosin-II regulation. *Curr. Opin. Cell Biol.* **11**, 26-33. doi:10.1016/S0955-0674(99)80004-0

Brown, J. M. and Garcia-Garcia, M. J. (2018). Secretory pathway calcium ATPase 1 (SPCA1) controls mouse neural tube closure by regulating cytoskeletal dynamics. *Development* **145**, dev170019.

Choi, W., Acharya, B. R., Peyret, G., Fardin, M. A., Mege, R. M., Ladoux, B., Yap, A. S., Fanning, A. S. and Peifer, M. (2016). Remodeling the zonula adherens in response to tension and the role of afadin in this response. *J. Cell Biol.* **213**, 243-260. doi:10.1083/jcb.201506115

Chu, C. W., Xiang, B., Ossipova, O., Ioannou, A. and Sokol, S. Y. (2018). The Ajuba family protein Wtip regulates actomyosin contractility during vertebrate neural tube closure. *J. Cell Sci.* **131**, jcs213884.

Colas, J. F. and Schoenwolf, G. C. (2001). Towards a cellular and molecular understanding of neurulation. *Dev. Dyn.* **221**, 117-145. doi:10.1002/dvdy.1144

Conti, M. A., Sellers, J. R., Adelstein, R. S. and Elzinga, M. (1991). Identification of the serine residue phosphorylated by protein kinase C in vertebrate nonmuscle myosin heavy chains. *Biochemistry* **30**, 966-970. doi:10.1021/bi00218a012

Coravos, J. S. and Martin, A. C. (2016). Apical sarcomere-like actomyosin contracts nonmuscle drosophila epithelial cells. *Dev. Cell* **39**, 346-358. doi:10.1016/j.devcel.2016.09.023

Dahan, I., Yearim, A., Touboul, Y. and Ravid, S. (2012). The tumor suppressor Lgl1 regulates NMII-A cellular distribution and focal adhesion morphology to optimize cell migration. *Mol. Biol. Cell* **23**, 591-601. doi:10.1091/mbc.e11-01-0015

Das, D., Zalewski, J. K., Mohan, S., Plageman, T. F., VanDemark, A. P. and Hildebrand, J. D. (2014). The interaction between Shroom3 and Rho-kinase is required for neural tube morphogenesis in mice. *Biol. Open* **3**, 850-860. doi:10.1242/bio.20147450

David, D. J., Tishkina, A. and Harris, T. J. (2010). The PAR complex regulates pulsed actomyosin contractions during amnioserosa apical constriction in Drosophila. *Development* **137**, 1645-1655. doi:10.1242/dev.044107

Dollar, G. L., Weber, U., Mlodzik, M. and Sokol, S. Y. (2005). Regulation of lethal giant larvae by Dishevelled. *Nature* **437**, 1376-1380. doi:10.1038/nature04116

Drees, F., Pokutta, S., Yamada, S., Nelson, W. J. and Weis, W. I. (2005). Alpha-catenin is a molecular switch that binds E-cadherin-beta-catenin and regulates actin-filament assembly. *Cell* **123**, 903-915. doi:10.1016/j.cell.2005.09.021

Du, T. T., Dewey, J. B., Wagner, E. L., Cui, R., Heo, J., Park, J. J., Francis, S. P., Perez-Reyes, E., Guillot, S. J., Sherman, N. E. et al. (2019). LMO7 deficiency reveals the significance of the cuticular plate for hearing function. *Nat. Commun.* **10**, 1117. doi:10.1038/s41467-019-09074-4

Dulyaninova, N. G., Malashkevich, V. N., Almo, S. C. and Bresnick, A. R. (2005). Regulation of myosin-IIA assembly and Mts1 binding by heavy chain phosphorylation. *Biochemistry* **44**, 6867-6876. doi:10.1021/bi0500776

Dulyaninova, N. G., House, R. P., Betapudi, V. and Bresnick, A. R. (2007). Myosin-IIA heavy-chain phosphorylation regulates the motility of MDA-MB-231 carcinoma cells. *Mol. Biol. Cell* **18**, 3144-3155. doi:10.1091/mbc.e06-11-1056

Ebrahim, S., Fujita, T., Millis, B. A., Kozin, E., Ma, X., Kawamoto, S., Baird, M. A., Davidson, M., Yonemura, S., Hisa, Y. et al. (2013). NMII forms a contractile transcellular sarcomeric network to regulate apical cell junctions and tissue geometry. *Curr. Biol.* **23**, 731-736. doi:10.1016/j.cub.2013.03.039

Eiraku, M., Takata, N., Ishibashi, H., Kawada, M., Sakakura, E., Okuda, S., Sekiguchi, K., Adachi, T. and Sasai, Y. (2011). Self-organizing optic-cup morphogenesis in three-dimensional culture. *Nature* **472**, 51-56. doi:10.1038/nature09941

Elliott, P. R., Irvine, A. F., Jung, H. S., Tozawa, K., Pastok, M. W., Picone, R., Badyal, S. K., Basran, J., Rudland, P. S., Barraclough, R. et al. (2012). Asymmetric mode of Ca(2)(+)-S100A4 interaction with nonmuscle myosin IIA generates nanomolar affinity required for filament remodeling. *Structure* **20**, 654-666. doi:10.1016/j.str.2012.02.002

Even-Faitelson, L. and Ravid, S. (2006). PAK1 and aPKCzeta regulate myosin II-B phosphorylation: a novel signaling pathway regulating filament assembly. *Mol. Biol. Cell* **17**, 2869-2881. doi:10.1091/mbc.e05-11-1001

Fanning, A. S., Jameson, B. J., Jesaitis, L. A. and Anderson, J. M. (1998). The tight junction protein ZO-1 establishes a link between the transmembrane protein occludin and the actin cytoskeleton. *J. Biol. Chem.* **273**, 29745-29753. doi:10.1074/jbc.273.45.29745

Fanning, A. S., Van Itallie, C. M. and Anderson, J. M. (2012). Zonula occludens-1 and −2 regulate apical cell structure and the zonula adherens cytoskeleton in polarized epithelia. *Mol. Biol. Cell* **23**, 577-590. doi:10.1091/mbc.e11-09-0791

Feng, J., Ito, M., Ichikawa, K., Isaka, N., Nishikawa, M., Hartshorne, D. J. and Nakano, T. (1999). Inhibitory phosphorylation site for Rho-associated kinase on smooth muscle myosin phosphatase. *J. Biol. Chem.* **274**, 37385-37390. doi:10.1074/jbc.274.52.37385

Garrett, S. C., Varney, K. M., Weber, D. J. and Bresnick, A. R. (2006). S100A4, a mediator of metastasis. *J. Biol. Chem.* **281**, 677-680. doi:10.1074/jbc.R500017200

Gorfinkiel, N. and Blanchard, G. B. (2011). Dynamics of actomyosin contractile activity during epithelial morphogenesis. *Curr. Opin. Cell Biol.* **23**, 531-539. doi:10.1016/j.ceb.2011.06.002

Haigo, S. L., Hildebrand, J. D., Harland, R. M. and Wallingford, J. B. (2003). Shroom induces apical constriction and is required for hingepoint formation during neural tube closure. *Curr. Biol.* **13**, 2125-2137. doi:10.1016/j.cub.2003.11.054

Harland, R. M. (1991). In situ hybridization: an improved whole-mount method for Xenopus embryos. *Methods Cell Biol.* **36**, 685-695. doi:10.1016/S0091-679X(08)60307-6

Hartsock, A. and Nelson, W. J. (2008). Adherens and tight junctions: structure, function and connections to the actin cytoskeleton. *Biochim. Biophys. Acta* **1778**, 660-669. doi:10.1016/j.bbamem.2007.07.012

Hashimoto, Y., Kinoshita, N., Greco, T. M., Federspiel, J. D., Jean Beltran, P. M., Ueno, N. and Cristea, I. M. (2019). Mechanical force induces phosphorylation-mediated signaling that underlies tissue response and robustness in Xenopus embryos. *Cell Syst* **8**, 226-241.e7. doi:10.1016/j.cels.2019.01.006

He, H., Li, W., Yan, P., Bundschuh, R., Killian, J. A., Labanowska, J., Brock, P., Shen, R., Heerema, N. A. and de la Chapelle, A. (2018). Identification of a recurrent LMO7-BRAF fusion in papillary thyroid carcinoma. *Thyroid* **28**, 748-754. doi:10.1089/thy.2017.0258

Heissler, S. M. and Sellers, J. R. (2014). Myosin light chains: teaching old dogs new tricks. *Bioarchitecture* **4**, 169-188. doi:10.1080/19490992.2015.1054092

Higashi, T., Arnold, T. R., Stephenson, R. E., Dinshaw, K. M. and Miller, A. L. (2016). Maintenance of the epithelial barrier and remodeling of cell-cell junctions during Cytokinesis. *Curr. Biol.* **26**, 1829-1842.

Hildebrand, J. D. (2005). Shroom regulates epithelial cell shape via the apical positioning of an actomyosin network. *J. Cell Sci.* **118**, 5191-5203. doi:10.1242/jcs.02626

Hildebrand, J. D. and Soriano, P. (1999). Shroom, a PDZ domain-containing actin-binding protein, is required for neural tube morphogenesis in mice. *Cell* **99**, 485-497. doi:10.1016/S0092-8674(00)81537-8

Hirano, S., Nose, A., Hatta, K., Kawakami, A. and Takeichi, M. (1987). Calcium-dependent cell-cell adhesion molecules (cadherins): subclass specificities and possible involvement of actin bundles. *J. Cell Biol.* **105**, 2501-2510. doi:10.1083/jcb.105.6.2501

Holaska, J. M., Rais-Bahrami, S. and Wilson, K. L. (2006). Lmo7 is an emerin-binding protein that regulates the transcription of emerin and many other muscle-relevant genes. *Hum. Mol. Genet.* **15**, 3459-3472. doi:10.1093/hmg/ddl423

Ibar, C., Kirichenko, E., Keepers, B., Enners, E., Fleisch, K. and Irvine, K. D. (2018). Tension-dependent regulation of mammalian Hippo signaling through LIMD1. *J. Cell Sci.* **131**, jcs214700. doi:10.1242/jcs.214700

Itoh, M., Nagafuchi, A., Yonemura, S., Kitani-Yasuda, T., Tsukita, S. and Tsukita, S. (1993). The 220-kD protein colocalizing with cadherins in non-epithelial cells is identical to ZO-1, a tight junction-associated protein in epithelial cells: cDNA cloning and immunoelectron microscopy. *J. Cell Biol.* **121**, 491-502. doi:10.1083/jcb.121.3.491

Itoh, M., Nagafuchi, A., Moroi, S. and Tsukita, S. (1997). Involvement of ZO-1 in cadherin-based cell adhesion through its direct binding to alpha catenin and actin filaments. *J. Cell Biol.* **138**, 181-192. doi:10.1083/jcb.138.1.181

Itoh, K., Ossipova, O. and Sokol, S. Y. (2014). GEF-H1 functions in apical constriction and cell intercalations and is essential for vertebrate neural tube closure. *J. Cell Sci.* **127**, 2542-2553. doi:10.1242/jcs.146811

Kowalczyk, I., Lee, C., Schuster, E., Hoeren, J., Trivigno, V., Riedel, L., Gorne, J., Wallingford, J. B., Hammes, A. and Feistel, K. (2021). Neural tube closure requires the endocytic receptor Lrp2 and its functional interaction with intracellular scaffolds. *Development* **148**, dev195008. doi:10.1242/dev.195008

Kurth, T. and Hausen, P. (2000). Bottle cell formation in relation to mesodermal patterning in the Xenopus embryo. *Mech. Dev.* **97**, 117-131. doi:10.1016/S0925-4773(00)00428-7

Lao, D. H., Esparza, M. C., Bremner, S. N., Banerjee, I., Zhang, J., Veevers, J., Bradford, W. H., Gu, Y., Dalton, N. D., Knowlton, K. U. et al. (2015). Lmo7 is dispensable for skeletal muscle and cardiac function. *Am. J. Physiol. Cell Physiol.* **309**, C470-C479. doi:10.1152/ajpcell.00177.2015

Lecuit, T., Lenne, P. F. and Munro, E. (2011). Force generation, transmission, and integration during cell and tissue morphogenesis. *Annu. Rev. Cell Dev. Biol.* **27**, 157-184. doi:10.1146/annurev-cellbio-100109-104027

Lin, Y. H., Zhen, Y. Y., Chien, K. Y., Lee, I. C., Lin, W. C., Chen, M. Y. and Pai, L. M. (2017). LIMCH1 regulates nonmuscle myosin-II activity and suppresses cell migration. *Mol. Biol. Cell* **28**, 1054-1065. doi:10.1091/mbc.e15-04-0218

Liu, X., Yuan, H., Zhou, J., Wang, Q., Qi, X., Bernal, C., Avella, D., Kaifi, J. T., Kimchi, E. T., Timothy, P. et al. (2021). LMO7 as an Unrecognized Factor Promoting Pancreatic Cancer Progression and Metastasis. *Front Cell Dev Biol* **9**, 647387. doi:10.3389/fcell.2021.647387

Manning, L. A., Perez-Vale, K. Z., Schaefer, K. N., Sewell, M. T. and Peifer, M. (2019). The Drosophila Afadin and ZO-1 homologues Canoe and Polychaetoid act in parallel to maintain epithelial integrity when challenged by adherens junction remodeling. *Mol. Biol. Cell* **30**, 1938-1960. doi:10.1091/mbc.E19-04-0209

Marlow, F., Topczewski, J., Sepich, D. and Solnica-Krezel, L. (2002). Zebrafish Rho kinase 2 acts downstream of Wnt11 to mediate cell polarity and effective convergence and extension movements. *Curr. Biol.* **12**, 876-884. doi:10.1016/S0960-9822(02)00864-3

Martin, A. C. and Goldstein, B. (2014). Apical constriction: themes and variations on a cellular mechanism driving morphogenesis. *Development* **141**, 1987-1998. doi:10.1242/dev.102228

Martin, A. C., Kaschube, M. and Wieschaus, E. F. (2009). Pulsed contractions of an actin-myosin network drive apical constriction. *Nature* **457**, 495-499. doi:10.1038/nature07522

Mason, F. M., Tworoger, M. and Martin, A. C. (2013). Apical domain polarization localizes actin-myosin activity to drive ratchet-like apical constriction. *Nat. Cell Biol.* **15**, 926-936. doi:10.1038/ncb2796

Merriam, R. W., Sauterer, R. A. and Christensen, K. (1983). A subcortical, pigment-containing structure in Xenopus eggs with contractile properties. *Dev. Biol.* **95**, 439-446. doi:10.1016/0012-1606(83)90045-3

Morita, H., Nandadasa, S., Yamamoto, T. S., Terasaka-Iioka, C., Wylie, C. and Ueno, N. (2010). Nectin-2 and N-cadherin interact through extracellular domains and induce apical accumulation of F-actin in apical constriction of Xenopus neural tube morphogenesis. *Development* **137**, 1315-1325. doi:10.1242/dev.043190

Mull, A., Kim, G. and Holaska, J. M. (2015). LMO7-null mice exhibit phenotypes consistent with emery-dreifuss muscular dystrophy. *Muscle Nerve* **51**, 222-228. doi:10.1002/mus.24286

Munjal, A., Philippe, J. M., Munro, E. and Lecuit, T. (2015). A self-organized biomechanical network drives shape changes during tissue morphogenesis. *Nature* **524**, 351-355. doi:10.1038/nature14603

Murakami, N., Chauhan, V. P. and Elzinga, M. (1998). Two nonmuscle myosin II heavy chain isoforms expressed in rabbit brains: filament forming properties, the effects of phosphorylation by protein kinase C and casein kinase II, and location of the phosphorylation sites. *Biochemistry* **37**, 1989-2003. doi:10.1021/bi971959a

Murphy, A. C. and Young, P. W. (2015). The actinin family of actin cross-linking proteins - a genetic perspective. *Cell Biosci* **5**, 49. doi:10.1186/s13578-015-0029-7

Nakajima, H. and Tanoue, T. (2011). Lulu2 regulates the circumferential actomyosin tensile system in epithelial cells through p114RhoGEF. *J. Cell Biol.* **195**, 245-261. doi:10.1083/jcb.201104118

Nakajima, H. and Tanoue, T. (2012). The circumferential actomyosin belt in epithelial cells is regulated by the Lulu2-p114RhoGEF system. *Small GTPases* **3**, 91-96. doi:10.4161/sgtp.19112
Nakamura, H., Hori, K., Tanaka-Okamoto, M., Higashiyama, M., Itoh, Y., Inoue, M., Morinaka, S. and Miyoshi, J. (2011). Decreased expression of LMO7 and its clinicopathological significance in human lung adenocarcinoma. *Exp. Ther. Med.* **2**, 1053-1057. doi:10.3892/etm.2011.329
Nieuwkoop, P. D. and Faber, J. (1967). *Normal Table of Xenopus laevis (Daudin). A Systematical and Chronological Survey of the Development from the Fertilized Egg till the End of Metamorphosis*, 2nd edn. Amsterdam, The Netherlands: North-Holland Publising Company.
Nishimura, T. and Takeichi, M. (2008). Shroom3-mediated recruitment of Rho kinases to the apical cell junctions regulates epithelial and neuroepithelial planar remodeling. *Development* **135**, 1493-1502. doi:10.1242/dev.019646
Ooshio, T., Irie, K., Morimoto, K., Fukuhara, A., Imai, T. and Takai, Y. (2004). Involvement of LMO7 in the association of two cell-cell adhesion molecules, nectin and E-cadherin, through afadin and alpha-actinin in epithelial cells. *J. Biol. Chem.* **279**, 31365-31373. doi:10.1074/jbc.M401957200
Ossipova, O. and Sokol, S. Y. (2021). Cryosectioning and Immunostaining of Xenopus Embryonic Tissues. *Cold Spring Harb Protoc* **2021**, pdb prot107151.
Ossipova, O., Kim, K., Lake, B. B., Itoh, K., Ioannou, A. and Sokol, S. Y. (2014). Role of Rab11 in planar cell polarity and apical constriction during vertebrate neural tube closure. *Nat. Commun.* **5**, 3734. doi:10.1038/ncomms4734
Ott, E. B., van den Akker, N. M., Sakalis, P. A., Gittenberger-de Groot, A. C., Te Velthuis, A. J. and Bagowski, C. P. (2008). The lim domain only protein 7 is important in zebrafish heart development. *Dev. Dyn.* **237**, 3940-3952. doi:10.1002/dvdy.21807
Peng, H. B. (1991). Xenopus laevis: practical uses in cell and molecular biology. Solutions and protocols. *Methods Cell Biol.* **36**, 657-662. doi:10.1016/S0091-679X(08)60301-5
Perez-Vale, K. Z. and Peifer, M. (2020). Orchestrating morphogenesis: building the body plan by cell shape changes and movements. *Development* **147**, dev191049. doi:10.1242/dev.191049
Popov, I. K., Ray, H. J., Skoglund, P., Keller, R. and Chang, C. (2018). The RhoGEF protein Plekhg5 regulates apical constriction of bottle cells during gastrulation. *Development* **145**, dev168922. doi:10.1242/dev.168922
Ramkumar, N., Omelchenko, T., Silva-Gagliardi, N. F., McGlade, C. J., Wijnholds, J. and Anderson, K. V. (2016). Crumbs2 promotes cell ingression during the epithelial-to-mesenchymal transition at gastrulation. *Nat. Cell Biol.* **18**, 1281-1291. doi:10.1038/ncb3442
Rauskolb, C., Sun, S., Sun, G., Pan, Y. and Irvine, K. D. (2014). Cytoskeletal tension inhibits Hippo signaling through an Ajuba-Warts complex. *Cell* **158**, 143-156. doi:10.1016/j.cell.2014.05.035
Razzell, W., Bustillo, M. E. and Zallen, J. A. (2018). The force-sensitive protein Ajuba regulates cell adhesion during epithelial morphogenesis. *J. Cell Biol.* **217**, 3715-3730. doi:10.1083/jcb.201801171
Roh-Johnson, M., Shemer, G., Higgins, C. D., McClellan, J. H., Werts, A. D., Tulu, U. S., Gao, L., Betzig, E., Kiehart, D. P. and Goldstein, B. (2012). Triggering a cell shape change by exploiting preexisting actomyosin contractions. *Science* **335**, 1232-1235. doi:10.1126/science.1217869
Royou, A., Sullivan, W. and Karess, R. (2002). Cortical recruitment of nonmuscle myosin II in early syncytial Drosophila embryos: its role in nuclear axial expansion and its regulation by Cdc2 activity. *J. Cell Biol.* **158**, 127-137. doi:10.1083/jcb.200203148
Salbreux, G., Charras, G. and Paluch, E. (2012). Actin cortex mechanics and cellular morphogenesis. *Trends Cell Biol.* **22**, 536-545. doi:10.1016/j.tcb.2012.07.001
Sawyer, J. K., Harris, N. J., Slep, K. C., Gaul, U. and Peifer, M. (2009). The Drosophila afadin homologue Canoe regulates linkage of the actin cytoskeleton to adherens junctions during apical constriction. *J. Cell Biol.* **186**, 57-73. doi:10.1083/jcb.200904001
Sawyer, J. K., Choi, W., Jung, K. C., He, L., Harris, N. J. and Peifer, M. (2011). A contractile actomyosin network linked to adherens junctions by Canoe/afadin helps drive convergent extension. *Mol. Biol. Cell* **22**, 2491-2508. doi:10.1091/mbc.e11-05-0411
Sawyer, J. M., Harrell, J. R., Shemer, G., Sullivan-Brown, J., Roh-Johnson, M. and Goldstein, B. (2010). Apical constriction: a cell shape change that can drive morphogenesis. *Dev. Biol.* **341**, 5-19. doi:10.1016/j.ydbio.2009.09.009
Schwayer, C., Sikora, M., Slovakova, J., Kardos, R. and Heisenberg, C. P. (2016). Actin Rings of Power. *Dev. Cell* **37**, 493-506. doi:10.1016/j.devcel.2016.05.024
Sherrard, K., Robin, F., Lemaire, P. and Munro, E. (2010). Sequential activation of apical and basolateral contractility drives ascidian endoderm invagination. *Curr. Biol.* **20**, 1499-1510. doi:10.1016/j.cub.2010.06.075
Shutova, M. S. and Svitkina, T. M. (2018). Mammalian nonmuscle myosin II comes in three flavors. *Biochem. Biophys. Res. Commun.* **506**, 394-402. doi:10.1016/j.bbrc.2018.03.103
Tanaka-Okamoto, M., Hori, K., Ishizaki, H., Hosoi, A., Itoh, Y., Wei, M., Wanibuchi, H., Mizoguchi, A., Nakamura, H. and Miyoshi, J. (2009). Increased susceptibility to spontaneous lung cancer in mice lacking LIM-domain only 7. *Cancer Sci.* **100**, 608-616. doi:10.1111/j.1349-7006.2009.01091.x
Tokuda, S., Higashi, T. and Furuse, M. (2014). ZO-1 knockout by TALEN-mediated gene targeting in MDCK cells: involvement of ZO-1 in the regulation of cytoskeleton and cell shape. *PLoS One* **9**, e104994. doi:10.1371/journal.pone.0104994
Van Itallie, C. M., Fanning, A. S., Bridges, A. and Anderson, J. M. (2009). ZO-1 stabilizes the tight junction solute barrier through coupling to the perijunctional cytoskeleton. *Mol. Biol. Cell* **20**, 3930-3940. doi:10.1091/mbc.e09-04-0320
Vicente-Manzanares, M., Ma, X., Adelstein, R. S. and Horwitz, A. R. (2009). Non-muscle myosin II takes centre stage in cell adhesion and migration. *Nat. Rev. Mol. Cell Biol.* **10**, 778-790. doi:10.1038/nrm2786
Wallingford, J. B., Niswander, L. A., Shaw, G. M. and Finnell, R. H. (2013). The continuing challenge of understanding, preventing, and treating neural tube defects. *Science* **339**, 1222002. doi:10.1126/science.1222002
Wei, Q. and Adelstein, R. S. (2000). Conditional expression of a truncated fragment of nonmuscle myosin II-A alters cell shape but not cytokinesis in HeLa cells. *Mol. Biol. Cell* **11**, 3617-3627. doi:10.1091/mbc.11.10.3617
Weiser, D. C., Row, R. H. and Kimelman, D. (2009). Rho-regulated myosin phosphatase establishes the level of protrusive activity required for cell movements during zebrafish gastrulation. *Development* **136**, 2375-2384. doi:10.1242/dev.034892
Williams, M., Burdsal, C., Periasamy, A., Lewandoski, M. and Sutherland, A. (2012). Mouse primitive streak forms in situ by initiation of epithelial to mesenchymal transition without migration of a cell population. *Dev. Dyn.* **241**, 270-283. doi:10.1002/dvdy.23711
Yamada, S., Pokutta, S., Drees, F., Weis, W. I. and Nelson, W. J. (2005). Deconstructing the cadherin-catenin-actin complex. *Cell* **123**, 889-901. doi:10.1016/j.cell.2005.09.020
Yonemura, S., Itoh, M., Nagafuchi, A. and Tsukita, S. (1995). Cell-to-cell adherens junction formation and actin filament organization: similarities and differences between non-polarized fibroblasts and polarized epithelial cells. *J. Cell Sci.* **108**, 127-142. doi:10.1242/jcs.108.1.127
Yu, H. H. and Zallen, J. A. (2020). Abl and Canoe/Afadin mediate mechanotransduction at tricellular junctions. *Science* **370**, eaba5528. doi:10.1126/science.aba5528
Yu-Kemp, H. C., Szymanski, R. A., Cortes, D. B., Gadda, N. C., Lillich, M. L., Maddox, A. S. and Peifer, M. (2022). Micron-scale supramolecular myosin arrays help mediate cytoskeletal assembly at mature adherens junctions. *J. Cell Biol.* **221**, e202103074.